

Article

Synthesis, Properties and Aging of ICP-CVD SiC_xN_y:H Films Formed from Tetramethyldisilazane

Maksim N. Chagin¹, Veronica S. Sulyaeva¹ , Vladimir R. Shayapov¹, Aleksey N. Kolodin², Maksim N. Khomyakov³, Irina V. Yushina¹ and Marina L. Kosinova^{1,*}

¹ Laboratory of Functional Films and Coatings, Nikolaev Institute of Inorganic Chemistry, SB RAS, 630090 Novosibirsk, Russia; chagin@niic.nsc.ru (M.N.C.); veronica@niic.nsc.ru (V.S.S.); shayapov@niic.nsc.ru (V.R.S.); jush@niic.nsc.ru (I.V.Y.)

² Laboratory of Extraction Processes, Nikolaev Institute of Inorganic Chemistry, SB RAS, 630090 Novosibirsk, Russia; kolodin.a.n@mail.ru

³ Laser Plasma Department, Institute of Laser Physics, SB RAS, 630090 Novosibirsk, Russia; mnkhomy@gmail.com

* Correspondence: marina@niic.nsc.ru

Abstract: Amorphous hydrogenated silicon carbonitride films were synthesized on Si(100), Ge(111), and fused silica substrates using the inductively coupled plasma chemical vapor deposition technique. 1,1,3,3-tetramethyldisilazane (TMDSN) was used as a single-source precursor. The effect of the precursor's pressure in the initial gas mixture, the substrate temperature, the plasma power, and the flow rate of nitrogen gas as an additional reagent on the film growth rate, element composition, chemical bonding, wettability of film surface, and the optical and mechanical properties of a-SiC_xN_y:H films was investigated. In situ diagnostic studies of the gas phase have been performed by optical emission spectroscopy during the film deposition process. The long-term stability of films was studied over a period of 375 days. Fourier-transform infrared (FTIR) and X-ray energy dispersive spectroscopy (EDX), and wettability measurements elucidated the oxidation of the SiC_xN_y:H films deposited using TMDSN + N₂ mixture. Films obtained from a mixture with argon had high stability and maintained the stability of element composition after long-term storage in ambient air.

Keywords: tetramethyldisilazane; silicon carbonitride; thin films; inductive coupling plasma chemical vapor deposition (ICP CVD); aging of films; film stability



Citation: Chagin, M.N.; Sulyaeva, V.S.; Shayapov, V.R.; Kolodin, A.N.; Khomyakov, M.N.; Yushina, I.V.; Kosinova, M.L. Synthesis, Properties and Aging of ICP-CVD SiC_xN_y:H Films Formed from Tetramethyldisilazane. *Coatings* **2022**, *12*, 80. <https://doi.org/10.3390/coatings12010080>

Academic Editor: Alexandru Enesca

Received: 10 December 2021

Accepted: 5 January 2022

Published: 11 January 2022

Publisher's Note: MDPI stays neutral with regard to jurisdictional claims in published maps and institutional affiliations.



Copyright: © 2022 by the authors. Licensee MDPI, Basel, Switzerland. This article is an open access article distributed under the terms and conditions of the Creative Commons Attribution (CC BY) license (<https://creativecommons.org/licenses/by/4.0/>).

1. Introduction

The unique properties of silicon carbide and silicon nitride materials are combined in Si–C–N compounds and can be tuned depending on the structure, composition, and chemical bonding in silicon carbonitride. Changing the parameters of the film synthesis makes this wide variation of properties possible. Low-temperature amorphous hydrogenated a-SiC_xN_y:H thin films and amorphous a-SiC_xN_y coatings were recognized several decades ago by researchers as important multi-functional materials [1–3]. The former has beneficial properties such as high transparency for ultraviolet-visible (UV-Vis) light, a low dielectric constant, and good environmental stability, while the latter has useful characteristics including high hardness and Young's modulus, excellent resistance to oxidation at a high temperature, and chemical inertness. These features make silicon carbonitride films suitable for a wide variety of applications such as low dielectric films, protective and hydrophobic coatings, blue-violet light-emitting diodes (LEDs) luminescent material, sensitive layers for sensors, and components of solar cells and optoelectronic devices [3–6].

At the present time, the deposition of silicon carbonitride films on the substrate surface is carried out by various physical (PVD) and chemical vapor deposition (CVD) techniques. Many of the known CVD methods are associated with certain implementational difficulties since they are based on the decomposition of silicon halides or silane and hydrocarbons

and carried out at high temperatures [2]. From this point of view, the use of organosilicon compounds as single-source precursors has become a significant step in the development of the film deposition processes [1]. These compounds have a number of important advantages such as incombustibility, non-toxicity, high volatility, and storage stability. It should be noted that precursor molecules have the all-necessary elements (silicon, nitrogen, and carbon) and contain Si–N, Si–C, and C–N bonds, which are incorporated into the films. The use of organosilicon single-source precursor greatly simplifies the technological process and CVD setup. Organosilicon compounds have a low boiling point and high vapor pressure at room temperature [1], which also simplifies the technological process since there is no need to heat pipelines. The earliest works on the use of organosilicon compounds in gas-phase deposition processes were conducted in the mid-70s, during the last century [7–11]. Since then, much effort has been directed towards studying “the composition-structure-property relationship” to develop processes for the synthesis of films with controlled functional characteristics. The final properties of the silicon carbonitride films are determined by the type of precursors and the reactions that take place in the gas phase and on the substrate surface, which are controlled by the type of gas-phase stimulation (temperature, plasma, and laser), the composition of the initial gas mixture, the ratio of reagents (precursor and additional gas), and the temperature of deposition processes. A large number of papers are known on the synthesis of silicon carbonitride films using 1,1,1,3,3,3-hexamethyldisilazane $[(\text{CH}_3)_3\text{Si}]_2\text{NH}$ (HMDSN) in mixtures with helium, nitrogen, hydrogen, or ammonia [1–3,10,12]. At the same time, on the basis of a review of publications, it can be concluded that there is limited work on the development and study of the processes of formation of $\text{SiC}_x\text{N}_y\text{:H}$ films during the decomposition of 1,1,3,3-tetramethyldisilazane $[(\text{CH}_3)_2\text{SiH}]_2\text{NH}$ (TMDSN).

The presence of the Si–H bond is a distinctive feature of TMDSN from HMDSN, which, as was found in [12], leads to an increase in the reactivity of this compound. Table 1 summarizes the data on the use of TMDSN as a precursor in various processes of chemical vapor deposition. Plasma-stimulated processes, which significantly reduce the temperature of film formation, were used in all cases. The deposition of films was carried out at both atmospheric and reduced pressure.

Table 1. Process parameters of $\text{SiC}_x\text{N}_y\text{:H}$ film deposition by decomposition of 1,1,3,3-tetramethyldisilazane and film functional characteristics.

Deposition Techniques	Deposition Conditions				Functional Properties			References
	Additional Gases	T_{dep} , °C	Plasma Frequency, Power	H, GPa E, GPa	n , max T, % E_g , eV	ϵ ρ , $\Omega \cdot \text{cm}$	CA, ° SFE, mN/m	
DP-CVD RPECVD	H ₂ N ₂ H ₂ + N ₂	30–400	2.45 GHz 120 W	5–31 30–210	1.45–2.00 – –	–	–	[12–21]
AP PECVD	N ₂ + He	25–450	13.56 MHz 140 W	0.5–15 20–142	1.5–2.0 – –	–	–	[22]
PECVD	He	100–700	27.12 MHz 60 W	3.8–36 21–190	1.5–2.6 88 2.5–5.0	3.8–4.6 2.2×10^{10}	–	[3,23]
RF PECVD	N ₂ NH ₃ N ₂ + NH ₃	50–300	–	–	1.61–2.29 90 2.38–3.33	–	–	[24,25]
ICP CVD	Ar Ar + N ₂	20–400	13.56 MHz 50–400 W	3.3–13.6 38.5–106	1.69–1.98 98 2.6–3.5	–	62–78 37–47	This study

T_{dep} , deposition temperature; H, hardness; E, Young’s modulus; n , refractive index; max T, maximum transparency value; E_g , band gap energy; ϵ , dielectric constant; ρ , resistivity; CA, contact angle; SFE, surface free energy; DP-CVD, direct plasma chemical vapor deposition; RPECVD, remote plasma enhanced chemical vapor deposition; AP PECVD, atmospheric pressure plasma enhanced chemical vapor deposition; RF PECVD, radio frequency plasma-enhanced chemical vapor deposition; ICP CVD, inductive coupling plasma chemical vapor deposition.

All developed plasma-chemical processes use co-reactants such as hydrogen, nitrogen, ammonia, helium, and their mixtures. The authors of [22] reported that film deposition using TMDSN occurs if there exists N_2 plasma in the deposition zone and there is no film formation without plasma or nitrogen (i.e., He plasma). At the same time, there are successful examples of using helium [3,23] and hydrogen plasma [18,19] for SiC_xN_y film growth. Much attention was paid to studying the effect of the parameters of the deposition processes, namely, the substrate temperature and the composition of the initial gas mixture, on the composition and chemical structure of the films. According to [20], with an increase in the deposition temperature, the IR spectra of the films change significantly: a marked rise in the intensity of the Si–C band, a decrease in the intensity of the Si–H, C–H, and Si–CH₂–Si/Si–O bands, a decay of the Si–CH₃ band intensity, a slight rise in the intensity of the N–H band, and an increase of the Si–N band intensity to a maximum at $T_{dep} = 100$ °C and then a drop for $T_{dep} > 100$ °C. All authors note that the silicon carbonitride films contain oxygen. The content of oxygen is about 12 at.% in the film (Rutherford backscattering spectroscopy data) and about 23 at.% on the film surface (X-ray photoelectron spectroscopy data) [20]. Wrobel's group [15,20] has reported a hypothetical mechanism of the most important elementary reactions contributing to the activation, growth, and crosslinking steps in SiC_xN_y film formation. These conclusions were drawn from the structural study and literature data. A limited number of works dealt with studies of the composition of the gas phase in plasma-enhanced processes of decomposition of organosilicon compounds. The papers [13,22] report on the study of the emission spectra of gas mixtures of $H_2 + N_2$ and $He + N_2$ that are used in the plasma-enhanced chemical vapor deposition (PECVD) processes with TMDSN. Optical emission spectroscopic analysis was used for the characterization of $HMDSN + N_2 + H_2 + Ar$ microwave plasma in [26].

With regard to the study of the functional properties of films, the main focus of the research was on the influence of the deposition conditions on the mechanical and optical properties of silicon carbonitride films. However, despite the long-term interest in the study of these layers, there are no data on the wettability and surface free energy of films obtained using TMDSN. The results obtained by Fainer et al. [3] showed that films had high optical transparency of up to 98% in the wavelength range of 280–2500 nm, which decreases with increasing deposition temperatures. According to Raman spectroscopy data, the high-temperature films ($T_{dep} > 400$ °C) had carbon clusters embedded in SiC_xN_y film that lowered the film transparency. The E_g value also decreases with an increase in the film synthesis temperature [21,23,24]. With an increase in the deposition temperature, the values of refractive index, hardness, and Young's modulus increase. This is associated with the change in the structure, chemical composition, and density of the a- $SiC_xN_y:H$ films. The films deposited at a lower temperature are soft and exhibit the presence of organic groups (Si–(CH₃)_n), while the a- SiC_xN_y that was deposited at a higher temperature forms hard, dense films consisting of Si–C and Si–N network [16,22,23]. Based on these data, it was concluded that, in the studied plasma-enhanced processes, deposition temperature plays a significant role in changing the physicochemical and functional properties of a- $SiC_xN_y:H$ films.

To determine the effect of the composition of the initial gas mixture on functional properties, Wrobel et al. used TMDSN + H_2 , TMDSN + N_2 , and TMDSN + $H_2 + N_2$ mixtures. The addition of nitrogen to the initial mixture worsened the mechanical and tribological properties and increased the roughness of the film surface. In mixtures with H_2 , the hardness of the films was 27–31 GPa and the coefficient of friction was minimum (0.04) [21].

No attention has been paid to the above-mentioned papers to study the long-term stability of a- $SiC_xN_y:H$ films produced in the PECVD processes with TMDSN. To date, there are relatively few studies devoted to the problem of aging processes and resistance to oxidation of a- $SiC_xN_y:H$ films that were deposited using other precursors. Authors [27] reported on the $SiC_xN_y:H$ film oxidation properties in the air at room temperature. The films were obtained by PECVD with $SiH_4 + CH_4 + NH_3 + H_2$ mixture at 240 °C. It was shown that the oxidation of the films occurred to a greater extent with increasing NH_3 flow rate.

In another study [28], PECVD films were deposited from $\text{SiH}_4 + \text{CH}_4 + \text{NH}_3 + \text{Ar}$ mixture in the temperature region of 200–400 °C. After several days, the appearance of a broad contribution from O–H stretching vibrations was found in IR spectra. The authors believe that the main reason for aging was a diffusion of ambient moisture, which affects layers deposited at lower temperatures more pronouncedly due to their higher degree of porosity. Plasma polymer coatings deposited by decomposition of 1,1,1,3,3,3-hexamethyldisilazane $[(\text{CH}_3)_3\text{Si}]_2\text{NH}$ were monitored as they aged in the air after fabrication in work [29]. The structure of this coating changed dramatically with aging: almost all silazane moieties disappeared per one year and a substantial amount of oxygen was incorporated, mainly in the form of siloxane links. The factors, features of the composition, and structure of the films affecting the oxidizing properties of a- $\text{SiC}_x\text{N}_y\text{:H}$ films are also rarely analyzed and discussed in publications. Taking into account the fact that the authors are considering films for wide environmental and industrial applications (optical devices, optoelectronics, corrosion protection, biomedical coatings, and others), the data on the stability of the composition of the films and their functional characteristics are necessary for further use.

It should be noted that tetramethyldisilazane has not previously been used as a precursor in the inductively coupled plasma chemical vapor deposition process (ICP CVD). Possessing an increased density and uniformity of the distribution of particles over the cross-section of the reactor, such a plasma provides greater uniformity of the films over the entire area of the substrate [30]. At low pressure and low deposition temperature, ICP CVD produces high-quality films such as $\text{SiN}_x\text{:H}$ [31,32], SiO_xN_y [33], $\text{SiO}_2/\text{SiN}_x$ film stacks [34], and $\text{SiC}_x\text{N}_y\text{:H}$ [35]. Previously, we used this technique for the synthesis of $\text{SiC}_x\text{N}_y\text{O}_z\text{:H}$ and $\text{SiC}_x\text{N}_y\text{:H}$ films by decomposition of hexamethyldisilazane and hexamethylcyclotrisilazane as precursors [36–38]. A similar synthetic approach was also used to prepare $\text{SiC}_x\text{:H}$ films by the decomposition of tetramethylsilane [39]. Due to the peculiarities of the ICP CVD process, the deposition parameters and the physicochemical properties of the films differed from those observed in conventional setups with external excitation of RF plasma and general heating of the growth zone. However, systematic studies of ICP CVD processes with TMDSN for the preparation of thin films of silicon carbonitride have not been carried out.

The present paper describes the ICP CVD synthesis of $\text{SiC}_x\text{N}_y\text{:H}$ thin films using 1,1,3,3-tetramethyldisilazane as a single-source precursor, argon as a gas-activator, and changes in chemical bonding and the composition of films, as well as optical, mechanical properties, the wettability of films with varying substrate temperatures, plasma power, and the addition of nitrogen gas. The study of the stability of the composition and properties of films is an important characteristic for discussing the prospects of their practical use. The results of studying the evolution of the composition of films during long-term storage will be presented below.

2. Experimental

2.1. Materials

Semiconducting n-type Si(100) wafers (KEF-4.5) of the dimensions of $10 \times 10 \times 0.47$ mm were used as substrates for Fourier transform infrared spectroscopy (FTIR), X-ray photoelectron spectroscopy (XPS), atomic force microscopy (AFM), scanning electron microscopy (SEM), ellipsometry, nanoindentation, and wettability investigations.

Ge(111) substrates ($10 \times 10 \times 0.2$ mm) were used for X-ray energy dispersive spectroscopy (EDX) analysis.

Fused silica plates of the dimensions $10 \times 10 \times 0.9$ mm were used as substrates for UV-Vis transmittance study.

Before being inserted into the reactor, all the substrates were degreased using trichloroethylene and acetone (high purity grade) and washed with deionized water. Then, the Si(100) substrates were chemically treated sequentially in ammonia-peroxide, hydrochloric-peroxide etchants, and in an HF solution. In the case of Ge(111) substrates, we used a solution of $\text{HNO}_3 + \text{HF} + \text{CH}_3\text{COOH}$ (3:4.5:9). Each stage was completed by washing with deionized water. The substrates were dried in a stream of nitrogen.

The precursor used in this study was 1,1,3,3-tetramethyldisilazane $[(\text{CH}_3)_2\text{SiH}]_2\text{NH}$ (97% purity) purchased from abcr GmbH & Co, KG, Wiesbaden, Germany.

Argon (high purity grade) and nitrogen (high purity grade) were used as gas-activator and additional reagents, respectively.

2.2. Film Growth

The film deposition was carried out in a CVD setup (Valiev Institute of Physics and Technology of the Russian Academy of Sciences, Moscow, Russia). These setups are based on optimized wide-aperture dense plasma sources with magnetic shielding of the reactor walls. Inductively coupled (13.56 MHz) discharge is used to generate process gas plasma. In the plasma processing zone, these ICP sources provide laterally homogeneous plasma with an ion density $n_i = (1-2) \times 10^{12} \text{ cm}^{-3}$ and an electron temperature $T_e \leq 3.5 \text{ eV}$ in the working pressure range $P = 1-20 \text{ mTorr}$. The ICP CVD system has been described in detail elsewhere [30,36,40]. Single-layer coatings were deposited under the following conditions: the residual pressure was 0.1 mTorr and the working pressure in the vacuum chamber was 3 mTorr. The films were deposited in Ar or Ar + N₂ atmosphere. The thickness of the films ranged from ~150 to ~400 nm. The properties of the films depend on deposition parameters. We studied the effect of the following parameters on the properties of films: the substrate temperature, the precursor's pressure, the plasma power, and the flow rates of the argon and nitrogen gases. Seven series of experiments were carried out by varying one parameter while maintaining the others constant. Table 2 summarizes the experimental conditions under which samples were obtained. For example, for all runs with variable temperature, the gas flow rate was fixed at 30 sccm and plasma power was equal to 200 W. In the case of the use of nitrogen/argon mixture, N₂ and Ar flow rates were varied together to keep the constant sum of the nitrogen and argon flows that was maintained to $30 \pm 1 \text{ sccm}$. For the convenience of describing gas mixtures simultaneously containing TMDSN, nitrogen, and argon, we introduced a value that describes the relative concentration of nitrogen in the gas mixture (the ratio of the nitrogen flow to the total flow of nitrogen and argon): $R(\text{N}_2) = F(\text{N}_2)/[F(\text{N}_2) + F(\text{Ar})]$, where $F(\text{N}_2)$ and $F(\text{Ar})$ are the flow rates of nitrogen and argon, respectively. Then, $R(\text{N}_2) = 1$ corresponds to the TMDSN + N₂ mixture and $R(\text{N}_2) = 0$ corresponds to the TMDS + Ar mixture.

Table 2. Experimental conditions of ICP CVD film growth.

Series	Addition Gas	$R(\text{N}_2) = F(\text{N}_2)/[F(\text{N}_2) + F(\text{Ar})]$	TMDSN Pressure, mTorr	Substrate Temperature, °C	Plasma Power, W
A	Ar	-	0.7–2	200	200
B	Ar	-	1	20–400	200
C	Ar	-	2	20–400	200
D	Ar	-	1	200	50–400
E	Ar	-	1	20–400	100
F	Ar + N ₂	0–1	1	300	200
G	Ar + N ₂	0–1	2	200	200

To study the stability of the films, two samples were deposited from different initial gas mixtures such as TMDSN + Ar and TMDSN + N₂. For the convenience of describing the research results, we denoted them as SiCN-A sample and SiCN-N sample. All other parameters of the deposition process were the same: the deposition temperature of 200 °C; plasma power of 200 W; the pressure of TMDSN in reactor chamber was 2 mTorr. Each series contained 16 samples that were prepared in one experiment in order to have identical specimens. The aging of the films was examined by exposing the samples to air environments. The samples were stored in cleaned plastic Petri dishes at room temperature and samples were not exposed to sources of UV radiation. The stability of samples was studied for more than 9000 h. We monitored the element composition, IR spectra, and wettability of the samples.

2.3. Film Characterization

The thickness and refractive index of the films were determined by variable angle monochromatic null ellipsometry using He-Ne laser at $\lambda = 632.8$ nm. The measurements were carried out at 5 incidence angles: 50° , 55° , 60° , 65° , and 70° . The ellipsometry inverse problem was solved using the model of one-layer film on the substrate (Si) with the known optical constants. The film thicknesses were further estimated and confirmed for some samples from cross-sectional view images acquired by SEM. The film growth rate was calculated by dividing film thickness by deposition time.

High-resolution images of the film surface were acquired using a field-emission scanning electron microscope JEOL JSM 6700F (Jeol, Tokyo, Japan) with the accelerated voltage of 5 keV in secondary electron mode. EDX elemental study was made using a Quantax 200 (Bruker, Berlin, Germany) analyzer for X-ray energy dispersive spectroscopy operating at 5 keV accelerated voltage.

Among spectroscopic methods, XPS, EDX, and FTIR spectroscopy are most commonly used to study the chemical composition and chemical bonding state of films. Raman spectroscopy is also very useful for monitoring the presence of carbon as an impurity phase in films.

The FTIR absorption spectra of the films were recorded using a SCIMITAR FTS 2000 (Digilab, Hopkinton, MA, USA) spectrometer in the wavenumber range of $375\text{--}4000\text{ cm}^{-1}$ with a resolution of 2 cm^{-1} . In each case, the background spectrum of the Si substrate was subtracted from that of the studied sample. For comparison of bonding intensities in all FTIR spectra, the absorbance value was normalized to the film's thickness.

Raman spectra were recorded on a LabRAM HR Evolution (Horiba, Kyoto, Japan) spectrometer equipped with a multichannel charge-coupled device (CCD) detector cooled with liquid nitrogen. The spectra were excited by a 632.8 nm He-Ne laser line with a power of about 1 mW on the sample surface. The spectral resolution of the spectrometer was established in the range of $2.4\text{--}3.8\text{ cm}^{-1}$.

The chemical properties of the surface samples were studied by applying XPS. Spectra were recorded on X-ray photoelectron spectrometer (SPECs Surface Nano Analysis GmbH, Berlin, Germany). The spectrometer is equipped with a PHOIBOS-150-MCD-9 hemispherical analyzer, an XR-50 X-ray source with a double Al/Mg anode, and an IQP-10/63 high energy ion source. The spectra were recorded using nonmonochromatized Al K_α radiation (1486.6 eV). The binding energy scales were referenced to 284.5 eV, as determined by the locations of the peak maxima of the C1s spectrum of a hydrocarbon. The relative concentrations of elements in the analysis zone were determined based on the integral intensities of XPS lines, taking into account the photoionization cross-sections of the corresponding terms [41]. For the detailed analysis of the chemical state of the elements, the regions of Si2p, C1s, N1s, and O1s core levels were surveyed and decomposed into individual components. Accordingly, after subtracting the background by the Shirley method [42], the experimental curve was expanded into several lines corresponding to the photoemission of electrons from atoms in different chemical environments. Data processing was carried out using the CasaXPS software package (version 2.3.24PR1.0) [43]. The shape of the peaks was approximated by a symmetric function obtained by multiplying the Gauss and Lorentz functions.

For the determination of film structure, XRD measurements were made by Shimadzu XRD-7000 diffractometer (Shimadzu, Kyoto, Japan) with the high-precision vertical $\theta\text{--}\theta$ goniometers, CuK_α radiation, and Ni filter. A range of scattering angles of $5^\circ < 2\theta < 60^\circ$ was covered with a step length of 0.03° and a count time of 1 s. The output beam size is 10×10 mm at a divergence angle of 0.22° .

The ICP CVD processes using TMDSN/argon/nitrogen gas mixture were investigated by optical emission spectroscopy. The chemical composition of ICP plasma was controlled with a "Kolibri-2" multichannel spectrometer (VMK "Optoelectronica", Novosibirsk, Russia) in the spectral range of $200\text{--}1200$ nm. The interpretation of the emission spectra was based on the literature data [44–46]. The figures presented below are for the range of

200–600 nm only, since the spectra have no additional information at higher wavelengths. Emission spectra were recorded for two values of discharge power at 200 and 400 W.

UV–Vis–NIR transmittance of the coatings was determined using Shimadzu UV-3101PC scanning spectrophotometer (Shimadzu, Kyoto, Japan) in the range of 190–3200 nm with a resolution of 2 nm. Absorption coefficient α was calculated from the transmission spectrum in the absorption edge, then optical band gap E_g was estimated using the Tauc's plot.

The measurements of the contact angles on the films were carried out on an OCA 15 PRO goniometer (Dataphysics, Filderstadt, Germany), equipped with a measuring video system with a USB camera, as well as a high-aperture measuring lens with an adjustable viewing angle. All measurements were carried out under normal conditions in a thermostated box ($T = 25 \pm 2$ °C, $P = 750$ Torr). The dosing needle diameter was 0.51 mm. Distilled water and diethylene glycol were used as test liquids. Surface tensions of the liquids with decomposition into dispersion and polar components are listed in Supplementary Materials (Table S1). The droplet volume was constant and amounted to ~ 2.5 μ L. The contact angles were measured in the sessile drop mode. The observed contact angle was calculated using Ellipse-Fitting and Young-Laplace algorithms. The contact angle data reported here were determined by averaging values measured at three different points on the surface of each sample. The calculation of the free surface energy (E_s , mN/m), as well as its polar and dispersion components (E_s^p and E_s^d), was carried out using three methods: Neumann, Owens–Wendt, and Wu [47–49]. For this, the values of the contact angles and surface tensions of two test liquids (water and diethylene glycol) with different polarities were used.

The mechanical properties, such as the hardness and Young's modulus of the films, were assessed by nanoindentation tests using a scanning nano-hardness tester NanoScan-3D (TISNCM, Troitsk, Moscow, Russia) with Berkovich diamond indenter (TISNCM, Troitsk, Moscow, Russia) at several loads in the range from 1 to 70 mN, with at least 10 indents being made for each load to reduce the effect of the random error.

The effect of aging on film properties was studied during more than 9000 h of storage in the air atmosphere. The changes in the properties of the films were monitored by ellipsometry, EDX, and FTIR spectroscopy.

3. Results and Discussion

The influence of the precursor's pressure (P) in the initial gas mixture, the deposition temperature (T_{dep}), and the plasma power (W) on the growth rate (V), element composition, chemical bonding, morphology, wettability of the film surface, and the optical and mechanical properties of the a-SiC_xN_y:H films are studied.

3.1. Film Growth Rate

An important stage in the development of the CVD process is the kinetic study for the subsequent precision control of the layer thickness. The film growth rate has been calculated by dividing the film thickness (ellipsometry measurements and SEM data) by deposition time. The deposition rate in the ICP CVD process was investigated with respect to dependence on TMDSN vapor pressure, deposition temperature, plasma power, and type of additional gases (Ar or Ar + N₂ mixture). All these parameters affect the film growth rate. Figure 1 shows the profiles of the film growth rates at the variable parameters of the deposition process. For samples of series A, the growth rate increases linearly from 16 to 80 nm/min with an increase in the vapor pressure of TMDSN in the reactor chamber in the range of 0.7–2 mTorr (Figure 1a). This is the expected result since an increase in the monomer flow increases the precursor's amount in the film deposition zone. The temperature dependences of the deposition rate of films for two values of TMDSN vapor pressure (1 and 2 mTorr) are plotted in Figure 1b (series B and C). The film growth rate decreases linearly despite the increase in substrate temperature.

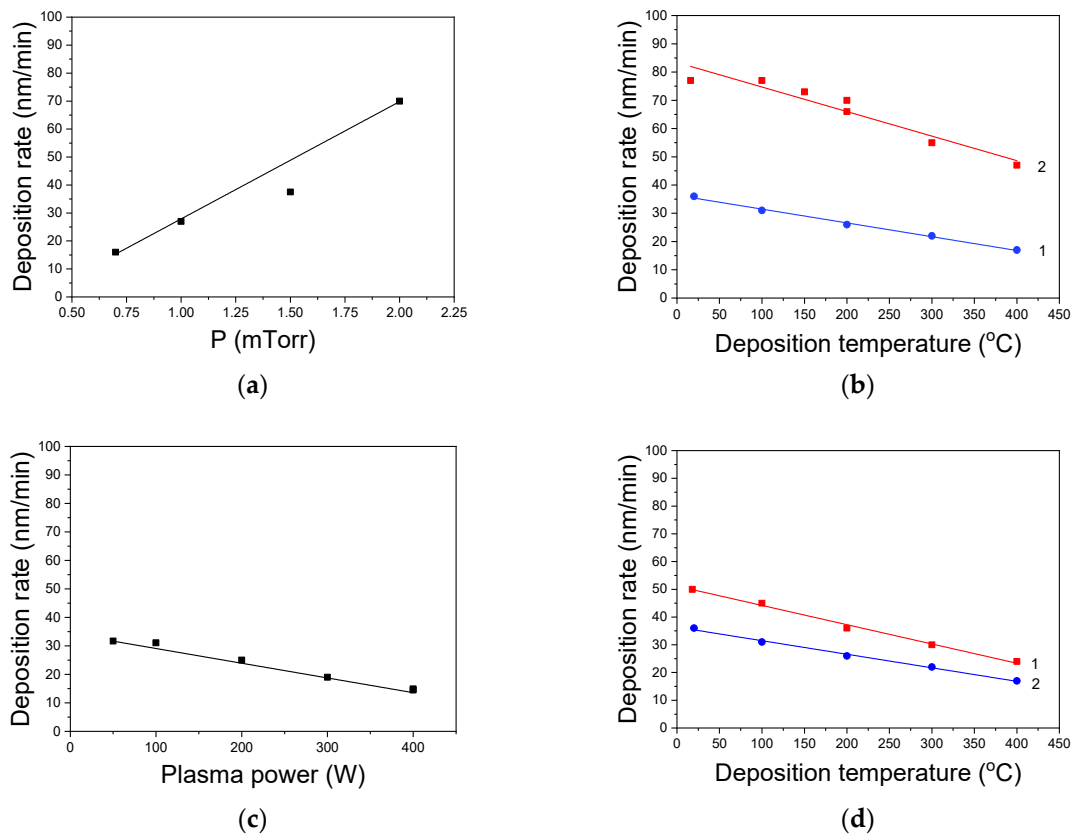


Figure 1. (a) Deposition rate of films versus TMSDN partial pressure (Series A); (b) Film growth rate as a function of the deposition temperature for TMSDN pressure of 1 mTorr (1) and 2 mTorr (2). (Series B and C); (c) Growth rate of films versus plasma power (Series D); (d) Temperature dependence of film growth rate for plasma power of 100 W (1) and 200 W (2). (Series E and B).

Similar results on a decrease in the deposition rate of films from the mixture of TMSDN + H₂ + N₂ were obtained in [17]. A decrease in the film growth rate with temperature in the PECVD process can result for various reasons: (a) high rate of desorption of reagents from the film surface due to higher substrate temperature; (b) premature decomposition of the precursor in the gas phase due to previous heating at a higher temperature in the hot-wall reactor and, as a result of this process, deplete the number of reagents available on the surface of the growing film; (c) compaction of high-temperature films. Figure 1c shows the effect of plasma power on the kinetic characteristics of the deposition process. By varying the plasma power from 50 to 400 W, the growth rate of the films decreases (series D). This may be associated with an increase in the etching of the growing film by active plasma species. The examples of the temperature dependence of the film growth rate at two values of plasma power (100 and 200 W) are present in Figure 1d.

Until now, there is no information on the effect of plasma power on the growth rate of films synthesized from TMSDN. In contrast to TMSDN, SiC_xN_y films deposited by the PECVD method using hexamethyldisilazane as a precursor and Ar as the feed gas, the growth rate was studied as a function of the applied RF plasma power of 100, 200, and 300 W [50]. A non-linear growth of the deposition rate with RF plasma power was observed.

Figure 2 shows the dependence of the film growth rate on the nitrogen content in the initial gas mixture for two values of the TMSDN partial pressure of 1 and 2 mTorr. The deposition rate increases slightly with the increasing nitrogen flow rate. This dependence agrees with information from the literature for plasma-stimulated processes, although significantly lower film growth rates (3–12 nm/min) were obtained in the RPCVD (2.45 GHz, 120 W) process using a mixture of TMSDN with H₂ and N₂ at 300 °C [13].

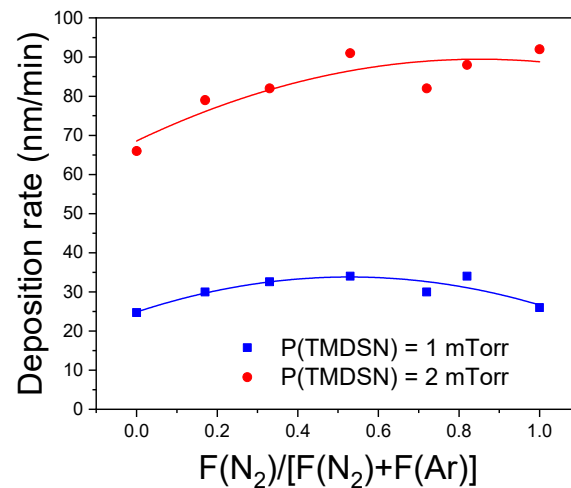


Figure 2. The growth rate of SiC_xN_y:H films deposited with various source gas ratios (F and G series).

3.2. Structure and Morphology Study

3.2.1. XRD Characterization

Figure S1 shows a typical XRD spectrum of SiC_xN_y:H film. A 210 nm thick film was deposited from TMDSN + Ar mixture at P(TMDSN) = 1 × 10^{−3} Torr, T_{dep} = 200 °C, and W = 200 W. The composition of this film, determined by the EDX method, was the following: [Si] = 24 at.%, [C] = 46 at.%, [N] = 23 at.%, and [O] = 7 at.%. This spectrum contains a wide diffuse halo and the only peak at 2θ = 33° corresponding to Si(200) reflection of substrate.

3.2.2. Surface Morphology Study

Scanning electron microscopy studies have shown that the films, regardless of their thickness, are typically continuous with a granular structure. Figure 3 depicts SEM images for films grown on Si(100) substrates at different N₂ flow rates. The films' surfaces are defect-free and exhibit a good morphological homogeneity. The increasing F(N₂) in ICP CVD processes leads to gran size decreasing from ≈30 to ≈15 nm but doesn't significantly change the film morphology and surface quality.

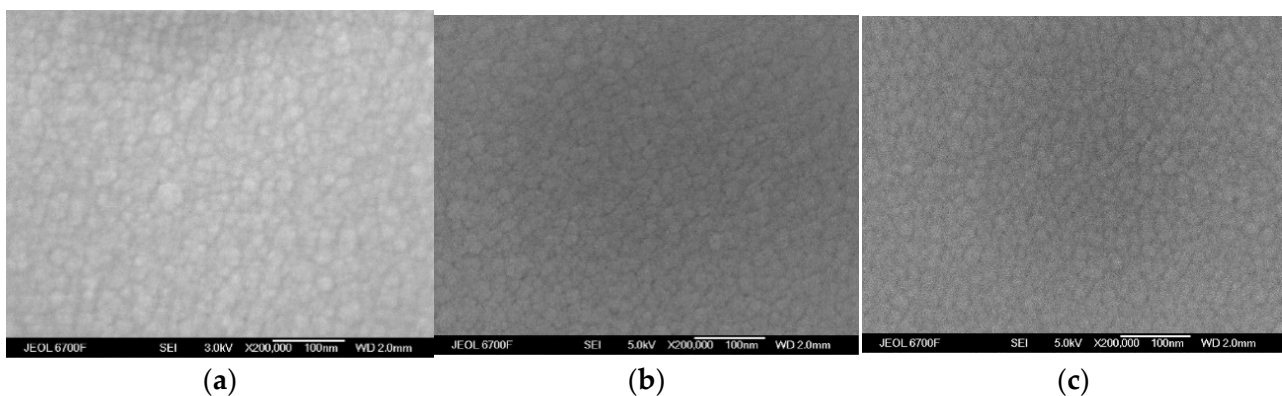


Figure 3. SEM images of SiC_xN_y:H deposited from TMDSN + N₂ mixture at F(N₂) = 0 (a), 15 (b), and 30 (c) sccm.

The cross-section view of the SiC_xN_y:H/Si(100) structure is presented in Figure 4. Based on this observation, it can be concluded that the SiC_xN_y:H film is homogeneous and defect-free. No discontinuities, cracks, or pores were detected.

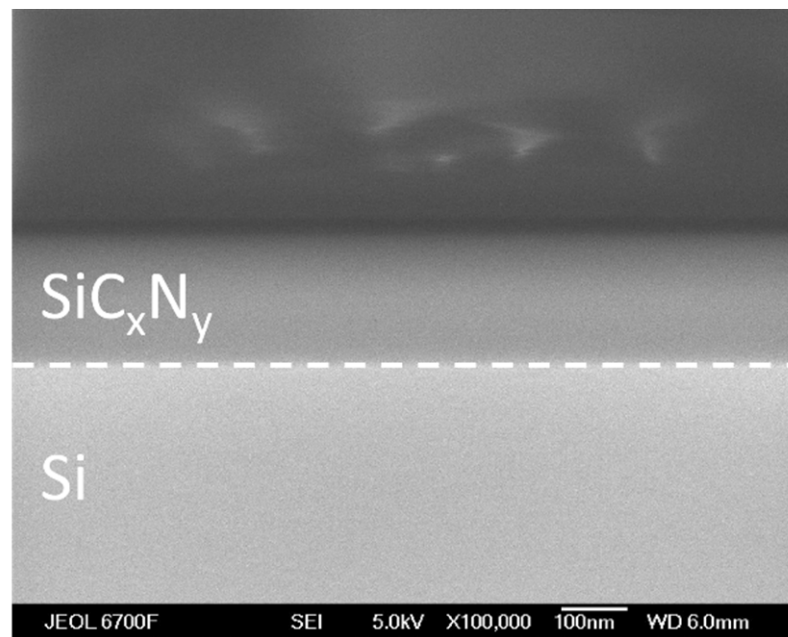


Figure 4. Cross-section SEM image of $\text{SiC}_x\text{N}_y\text{:H}/\text{Si}(100)$ structure. The film deposition conditions: $T_{\text{dep}} = 200\text{ }^\circ\text{C}$, $W = 200\text{ W}$, $F(\text{Ar}) = 30\text{ sccm}$, $F(\text{N}_2) = 0\text{ sccm}$.

3.3. Chemical Composition of $\text{SiC}_x\text{N}_y\text{:H}$ Films

3.3.1. EDX Data

Energy-dispersive X-ray spectroscopy (EDX) is an analytical tool used for the chemical characterization (elemental analysis) of thin film samples. EDX is based on the emission X-ray signal from the bulk sample due to primary electron beam bombardment. All studied samples contained silicon, carbon, nitrogen, and oxygen as the main elements. There are several reasons for oxygen contamination of films. Firstly, it may be not a high vacuum in the reactor chamber and, secondly, it is the effect of atmospheric oxygen and/or moisture on the film surface during storage in the air after growth.

Figure 5a shows the dependence of the element composition of films on TMDSN pressure (samples of series A). The content of carbon and silicon increases slightly, while the content of nitrogen decreases with an increase in the partial pressure of the precursor in the initial gas mixture. The temperature dependence of the composition of the films shown in Figure 5b (series C) indicates a very weak increase in the silicon and carbon content and a decrease in the nitrogen content. Moreover, at temperatures above $200\text{ }^\circ\text{C}$, the composition of the films is practically constant. We also observed similar weak temperature dependence of the composition of the films during the synthesis of $\text{SiC}_x\text{:H}$ and $\text{SiC}_x\text{N}_y\text{:H}$ films from organosilicon compounds in the process of ICP CVD [36,39]. In contrast to our work, the authors [23] who studied the process of obtaining films from a mixture of TMDSN with helium in the PECVD process determined that with an increase in the deposition temperature from 100 to $700\text{ }^\circ\text{C}$, the silicon content significantly increases, the carbon content decreases, and the amount of nitrogen remains approximately constant.

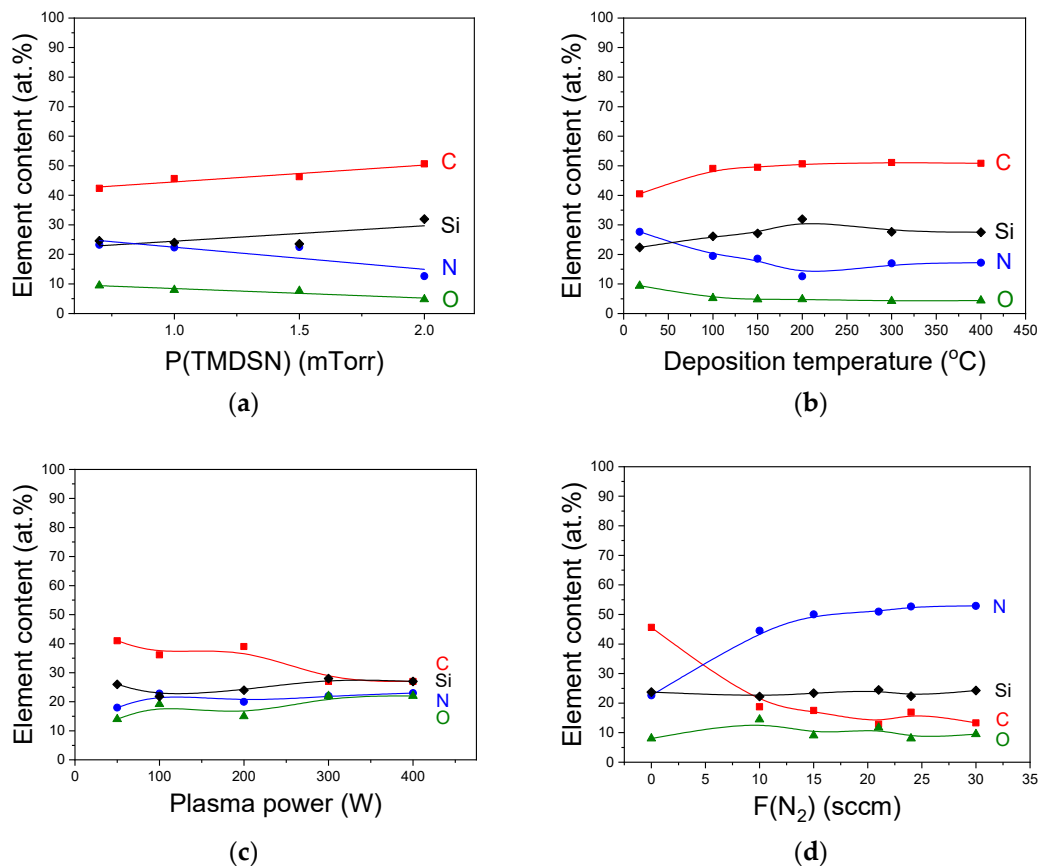


Figure 5. Elemental composition of SiC_xN_y:H films depending on TMSDN pressure (a); deposition temperature (b); plasma power (c); and nitrogen flow rate (d).

Silicon carbonitride thin films have been investigated for element composition as a function of the RF plasma power in the range of 50–400 W (series D, Figure 5c). With an increase in plasma power, the carbon content decreases and the content of other elements changes insignificantly. It should be noted that adding nitrogen into the gas mixture has a significant effect on the composition of the films. Figure 5d shows the atomic concentration of elements for the films deposited at F(N₂) = 0–30 sccm (series F). One can see that Si content is rather constant (23–24 at.%), whereas the content of carbon and nitrogen changes considerably. Indeed, carbon content decreases from 45 at.% to 13 at.%, and nitrogen content increases from 22 at.% to 54 at.%.

3.3.2. Film Chemical Bonding State

When analyzing the IR spectra of a-SiC_xN_y:H films, the determination of absorption peaks is a difficult and often controversial task due to many possible bonds and terminating groups. The IR spectra of all samples grown on Si(100) substrates were recorded to study the composition and chemical structure of the synthesized films. The Si(100) substrate after standard chemical treatment was used as a reference sample. The magnitude of the peaks was normalized to the film thickness. The SiC_xN_y:H films deposited using both TMSDN + Ar and TMSDN + N₂/Ar mixtures were studied and compared with the IR absorption spectra of TMSDN precursor (Figure 6 and Table 3). The interpretation of the spectra (the identification of certain absorption bands) was based on the literature data [51–55]. Si–NH–Si group has absorption at 3385 cm^{−1} from the N–H stretching modes. The NH deformation and bending vibrations give the bands at 1518 cm^{−1} and 1173 cm^{−1}, respectively. Si–N–Si symmetric stretching vibration shows a band at 927 cm^{−1}. The Si–CH₃ group is recognized by the band at 1250 cm^{−1} due to the symmetric –CH₃ deformation, together with bands in the range 865–750 cm^{−1}. The methyl group has two bands at 2958

and 2900 cm^{-1} corresponding to antisymmetric and symmetric stretching vibrations. The Si–H vibrational mode shows a very strong band at 2117 cm^{-1} .

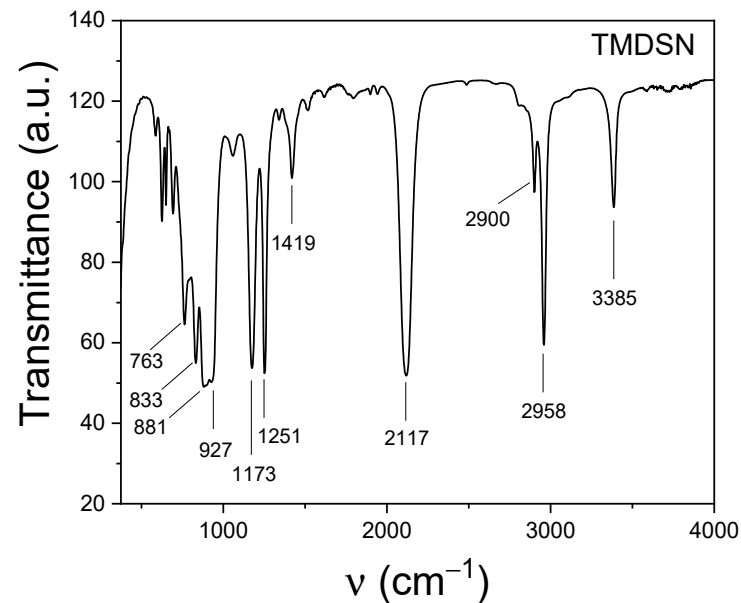


Figure 6. FTIR spectrum of TMDSN precursor.

Table 3. Band assignment of TMDSN FTIR spectrum.

TMDSN		
Peak Position (cm^{-1})	Assignment	Structural Fragment
3385	$\nu(\text{NH})$	Si–NH–Si
2958	$\nu_a(\text{CH})$	CH_3
2900	$\nu_s(\text{CH})$	CH_3
2117	$\nu(\text{SiH})$	SiH
1518	$\delta(\text{NH})$	Si–NH–Si
1419	$\delta_a(\text{CH})$	CH_3
1250	$\delta_s(\text{CH})$	Si– CH_3
1173	$\delta(\text{NH})$	Si–NH–Si
927	$\nu_s(\text{Si–N–Si})$	Si–NH–Si
881	$\delta(\text{CH})$	Si(CH_3) ₂
833	$\rho(\text{CH})$	Si(CH_3) ₂
763	$\nu(\text{SiC})$	–Si–C–

Vibrational modes: ν , δ , and ρ denote stretching, bending, and rocking modes, respectively. Subscripts a and s denote asymmetric and symmetric vibrations.

Figure 7a illustrates the evolution of the FTIR spectra with deposition temperature for films grown from TMDSN + Ar mixture (series C). For all films, the characteristic area is a wide main band at the wavenumbers of $1300\text{--}700\text{ cm}^{-1}$. It should be noted that the spectrum of the film obtained at the lowest deposition temperature (room temperature) differs from the other spectra. Figure 7c presents the main band, which, as can be assumed, corresponds to the superposition of the following bands: C–H deformation mode in Si– CH_3 groups (1262 cm^{-1}), N–H bending mode of Si–NH–Si and/or C–N (1153 cm^{-1}), Si–O stretching mode (1106 cm^{-1}), CH_2 wagging mode of Si– CH_2 –Si and/or Si–O stretching mode (1030 cm^{-1}), Si–N stretching mode (931 cm^{-1}), and Si–C stretching mode (819 cm^{-1}). The band at 3370 cm^{-1} is associated with N–H stretching. The wide peak in the region of $3000\text{--}2760\text{ cm}^{-1}$ is an overlap of several asymmetric and symmetric stretches of CH_n groups. Another wide peak in the region of $2300\text{--}2070\text{ cm}^{-1}$ is assigned a superposition

of the absorption Si–H (2113 cm^{-1}) and $\text{C}\equiv\text{N}$ (2180 cm^{-1}) stretching vibrations. The absorption band around 1650 cm^{-1} is associated with $\text{C}=\text{N}/\text{C}=\text{C}$ bond vibrations. Figure 7b presents the temperature dependence of the intensity of Si–C, Si–N, Si–CH₂–Si/Si–O, and Si–NH–Si/C–N peaks. With an increase in deposition temperature, the intensity of the Si–C band immediately increases and, crossing $200\text{ }^{\circ}\text{C}$, its value becomes constant; at the same time, the intensities of Si–N, Si–CH₂–Si/Si–O, and Si–NH–Si/C–N peaks do not change extensively, only slightly decreasing.

As the temperature increases to $400\text{ }^{\circ}\text{C}$, the maximum of the base band is shifted to the region of lower frequencies. The deconvoluted IR absorption band for $\text{SiC}_x\text{N}_y\text{:H}$ film deposited at $400\text{ }^{\circ}\text{C}$ is presented in Figure 7d, where the main band is associated with vibrations of the Si–C (818 cm^{-1}), Si–N (949 cm^{-1}), Si–CH₂–Si/Si–O (1028 cm^{-1}), Si–NH–Si/C–N (1160 cm^{-1}), and C–H (1254 cm^{-1}) bonds. The increase of the substrate temperature from 20 to $400\text{ }^{\circ}\text{C}$ causes the elimination of NH and $\text{C}=\text{N}/\text{C}=\text{C}$ groups from the films. The position, shape, and intensity of the bands associated with vibrations of CH_n , Si–H, and Si–CH₃ groups are practically independent of the deposition temperature. This result differs from the data of other authors, who noted a significant drop in the intensity of the absorption band arising from the C–H stretching mode with rising T_{dep} [20].

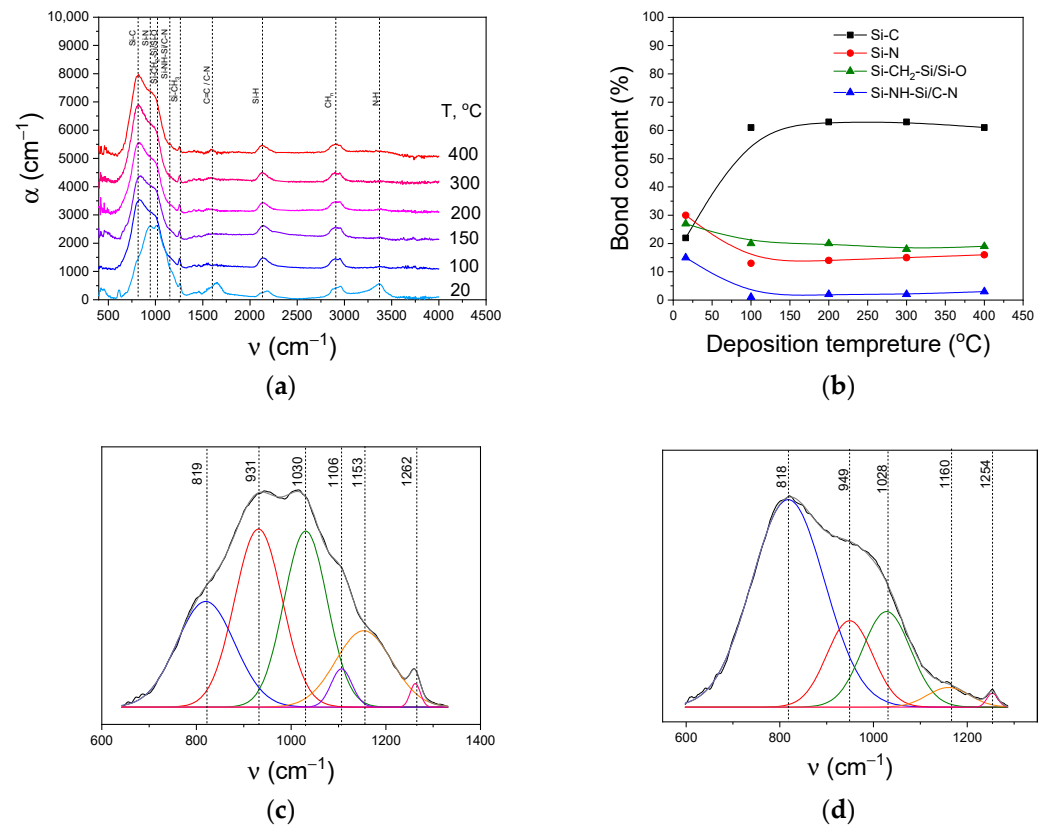


Figure 7. (a) Evolution of FTIR spectra of $\text{SiC}_x\text{N}_y\text{:H}$ films produced at different deposition temperature (Series C); (b) The relative integrated intensities of the IR bands from the Si–N, Si–C, and Si–CH₂–Si/Si–O units. Result of deconvolution into Gaussian profiles of the absorption band in the range of $1400\text{--}700\text{ cm}^{-1}$ for $\text{SiC}_x\text{N}_y\text{:H}$ films deposited at $20\text{ }^{\circ}\text{C}$ (c) and $400\text{ }^{\circ}\text{C}$ (d).

Figure 8a shows the FTIR spectra of the $\text{SiC}_x\text{N}_y\text{:H}$ films deposited at various nitrogen contents in the Ar–N₂ mixture. There is an intense broad absorption band in the range of $1300\text{--}500\text{ cm}^{-1}$ in all the spectra of the films. It should be noted that the shape of this band changes with an increase in the nitrogen content in the gas mixture. Deconvolution of the main band of the spectra of films synthesized without and with the addition of nitrogen is shown in Figure 8c,d. In the first case, the band includes overlapping signals from the CH₃ deformation mode of Si–CH₃ groups (1257 cm^{-1}), N–H bending mode of Si–NH–Si

and/or C–N (1172 cm^{-1}), the Si–O stretching mode and/or $-\text{CH}_2-$ wagging mode of Si–CH₂–Si (1028 cm^{-1}), the Si–N stretching mode (942 cm^{-1}), and the Si–C stretching mode (821 cm^{-1}). In the second case, the intensity of the nitrogen-containing bands at 1179 cm^{-1} and 917 cm^{-1} increases. Figure 8b shows the change in the intensity of Si–C and Si–N peaks with an increase in the nitrogen flow rate. Even with a small addition of nitrogen, the intensity of the Si–C peak drops sharply, while the intensity of the Si–N peak increases. The most notable difference in the spectra of the film deposited with using only argon and films deposited with Ar + N₂ mixture concerns the peaks in the ranges of 3357 cm^{-1} (N–H stretching mode), 2190 cm^{-1} (C≡N stretching mode, Si–H stretching mode), 1620 cm^{-1} (C=N/C=C), and 1179 cm^{-1} (N–H bending mode), the intensity of which increases with increasing nitrogen flow rate. Thus, as the N₂ content of the feed gas mixture increases, significant changes in absorption characteristics are noted. Comparing Figures 5, 7 and 8, it can be seen that the data of EDX and FTIR spectroscopy are in good agreement.

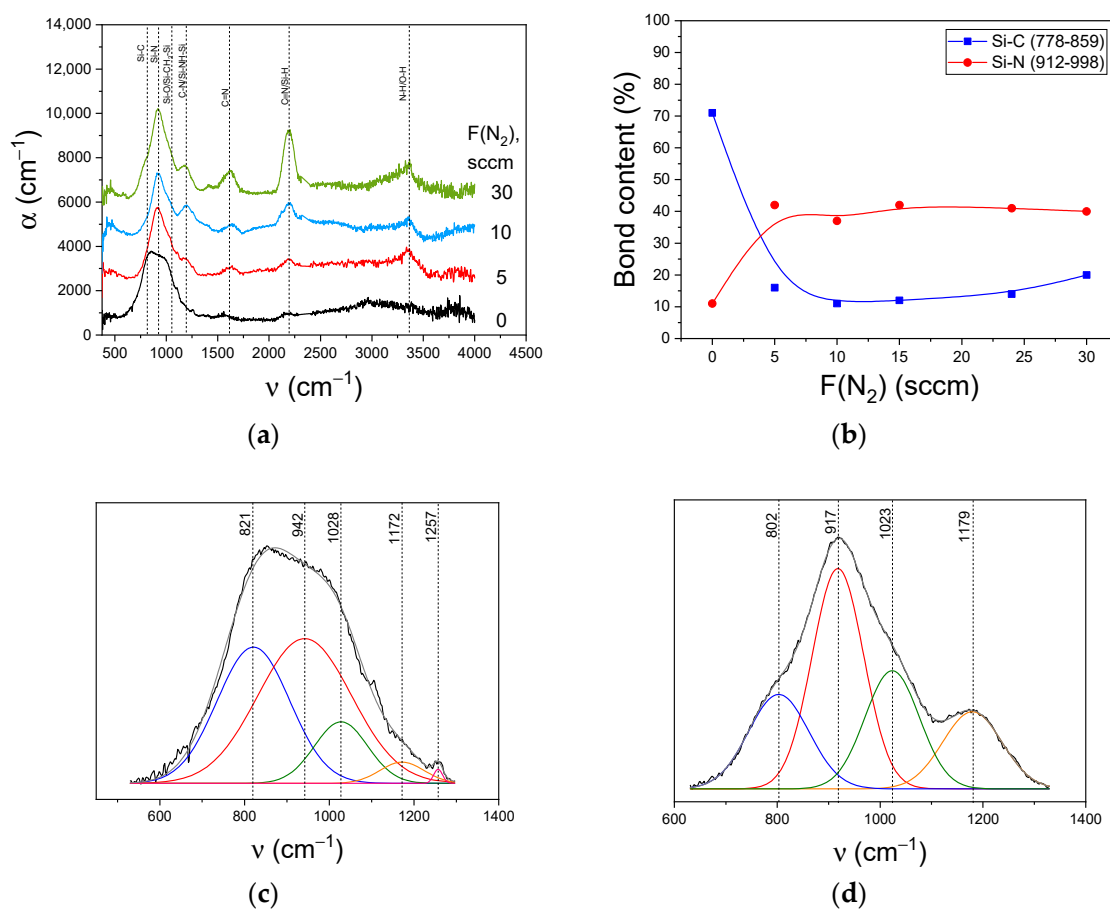


Figure 8. (a) Evolution of FTIR spectra of SiC_xN_y:H films produced at a different nitrogen flow rate (Series F); (b) The relative integrated intensities of the IR bands from the Si–N and Si–C units. Result of deconvolution into Gaussian profiles of the absorption band in the range of 1300–600 cm^{-1} for SiC_xN_y:H films deposited at F(N₂) = 0 (c) and 30 sccm (d).

3.3.3. Raman Spectroscopy

In this work, we recorded and studied the Raman spectra of all samples obtained under various synthesis conditions on Si(100) substrates. All spectra contained a single maximum at 520 cm^{-1} , related to the vibrations of monocrystalline silicon. The absence of D and G bands in the region of 1340 and 1580 cm^{-1} , characteristic of disordered graphite clusters [56], indicates their absence in the films.

3.3.4. Chemical Composition by XPS

Further confirmation of the chemical structure (local bonding environment) of $\text{SiC}_x\text{N}_y\text{:H}$ films was obtained using XPS. For this study, three samples of series F were selected, synthesized at the temperature of 300 °C, the plasma power of 200 W, $P(\text{TMDSN}) = 1$ mTorr, and at various values of the nitrogen flow rate of 0, 15, and 30 sccm that were depicted as F-0, F-15, and F-30, respectively. XPS results for the films deposited from both the TMDSN + Ar and TMDSN + N_2/Ar mixtures indicate the presence of Si, C, N, and O atoms. Table 4 presents the relative concentrations (atomic ratios) of elements in the near-surface layer of the samples and their comparison with EDX data. It is evident that an increase in the nitrogen flow rate leads to an increase in its concentration in the films. The dependence of change in element content acquired by XPS and EDX has the same tendency, with the exception that XPS data shows the presence of more carbon and oxygen content due to surface hydrocarbon contaminations. Figure 9 shows the $\text{Si}2p$, $\text{C}1s$, and $\text{N}1s$ core-level spectra. The asymmetric shape of peaks indicates the presence of these atoms in different chemical environments. To analyze these spectra, the curve-fit analysis was performed. Table 5 shows the obtained values of the binding energies.

Table 4. Element composition of $\text{SiC}_x\text{N}_y\text{:H}$ films. For comparison, the EDX data in parentheses are given.

Samples	F(N_2), sccm	Element Composition			
		Si, at. %	C, at. %	N, at. %	O, at. %
F-0	0	27 (26)	43 (38)	14 (24)	16 (10)
F-15	15	29 (27)	15 (12)	28 (49)	28 (11)
F-30	30	29 (27)	15 (10)	32 (55)	24 (6)

Table 5. Fine structure of the XPS spectra for $\text{Si}2p$, $\text{C}1s$, and $\text{N}1s$ core levels.

Sample	E_b , eV (Content, %)								
	$\text{Si}2p$			$\text{C}1s$				$\text{N}1s$	
	Si–O	Si–N	Si–C	C–O	C–N	C–C	C–Si	N–C	N–Si
F-0	102.7 (18%)	101.7 (63%)	100.8 (19%)	288.0 (2%)	285.7 (11%)	284.6 (61%)	283.7 (26%)	399.8 (12%)	397.3 (88%)
F-15	102.8 (28%)	101.7 (66%)	100.8 (6%)	287.9 (11%)	286.1 (21%)	284.4 (67%)	283.1 (2%)	399.5 (14%)	397.5 (86%)
F-30	102.7 (25%)	101.5 (70%)	100.9 (6%)	287.5 (16%)	285.9 (26%)	284.4 (57%)	282.9 (2%)	399.5 (15%)	397.4 (85%)

The $\text{Si}2p$ spectrum of the film obtained without the nitrogen addition (F-0 sample) can be fitted to three components at 100.8, 101.7, and 102.7 eV. The most intense peak at 101.7 eV corresponds to silicon atoms predominantly bonded to nitrogen atoms. The $\text{N}1s$ spectrum has a complimentary strong component at 397.3 eV. Two other peaks at 100.7 and 102.7 eV can be attributed to silicon atoms bonded to carbon and oxygen atoms. There is no shift in the $\text{Si}2p$ spectra at the addition of nitrogen to the gas phase. The intensity of the component of $\text{Si}2p$ peak at 101.5–101.7 eV (Si–N) increases slightly, while the component at 100.8–100.9 eV (Si–C) decreases. Simultaneously, the component of $\text{C}1s$ peak corresponding to C–Si bonding also decreases, and the intensity of the N–C component at 399.5–399.8 eV increases slightly. It should be noted that with an increase in the nitrogen content in the gas phase, the intensity of the 102.7–102.8 eV peak corresponding to SiO_x species increases. A similar trend takes place for $\text{C}1s$ peak at 287.5–288.0 eV due to carbonate or carboxylic groups. These data indicate that the surface of F-15 and F-30 samples are more oxidized. It should be emphasized that all spectra showed a peak at 284.4–284.6 eV, which can be attributed to sp^2 -hybridized carbon.

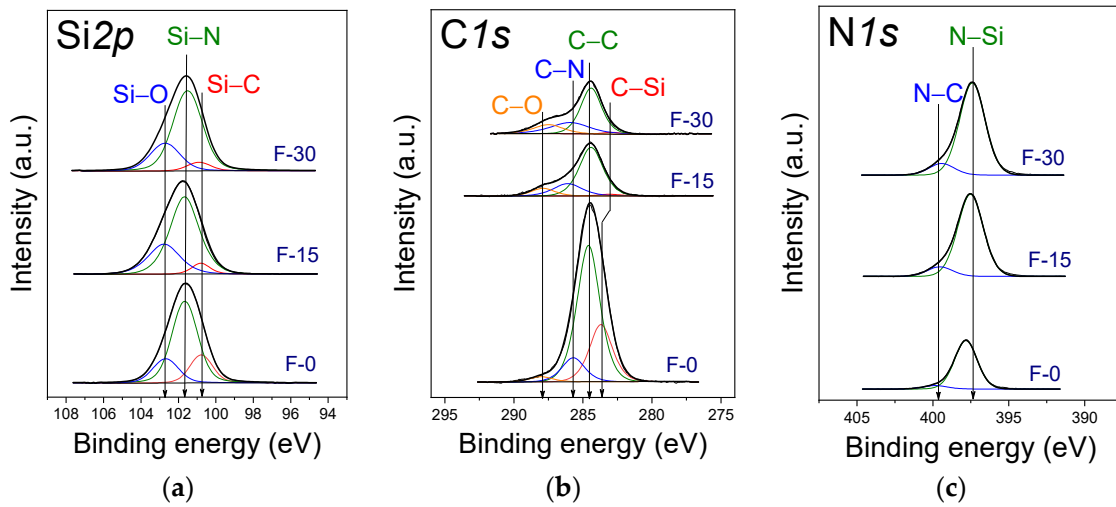


Figure 9. Si2p (a), C1s (b), and N1s (c) spectra of a-Si_xN_y:H films.

3.4. Gas Phase Composition

Figure 10 shows the emission spectrum of the plasma generated by the ICP source (200 W) in the Ar-N₂ mixture at R(N₂) = 0.54. The most important spectral features have been indicated in the graphs. This spectrum possesses intense nitrogen (N₂) molecular bands, cyano (CN) free radical bands, C₂ dimer bands, hydrogen, and silicon atomic lines.

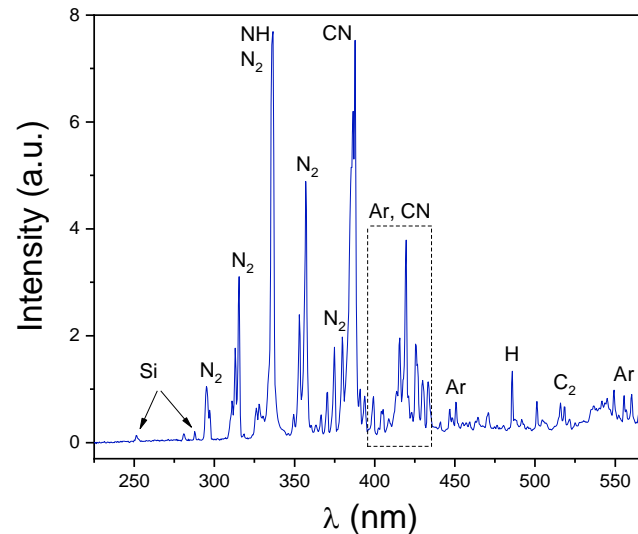


Figure 10. Optical emission spectrum from the TMDSN + Ar + N₂ plasma. The spectrum has been measured on ICP CVD reactor with 200 W plasma power, 30 sccm total flow, R(N₂) = 0.54, and P(TMDSN) = 1 mTorr.

To reveal the regularities that occur under varying of the initial gas mixture composition, the dependences of the intensities of the argon line at 763.5 nm, the nitrogen molecular band at 357.7 nm, the silicon line at 288.2 nm, the C₂ band at 516.5 nm, the H_α hydrogen line at 656.3 nm and CN band at 386.5 nm were plotted versus R(N₂) (Figure 11). A similar dependence of the intensity of the hydrogen atomic line on the nitrogen concentration in the N₂ + H₂ mixture was observed in [13]. The intensities of the argon line and N₂ band correlate quite well with the changes in the composition of the initial gas mixture. The intensities of the silicon line and the C₂ band decrease with an increase of nitrogen content in the initial gas mixture. The intensity of the H_α hydrogen line remains almost unchanged till R(N₂) < 0.7, and it decreases at a higher nitrogen concentration. The intensity of the CN band increases sharply with an increase in the nitrogen concentration when R(N₂) = 0–0.5 and reaches

the plateau at $R(N_2) \sim 0.5$ (Figure 11). The intensity of this band slightly decreases at $R(N_2) = 1$. Similar regularities were obtained for the tetramethylsilane + N_2 + Ar gas mixture in [57] and an assumption was made that argon atoms activate the decomposition of tetramethylsilane molecules via the Si–C bond breaking rather than the C–H bond. It can be expected that a similar mechanism exists in the case of TMDSN. In addition, our results show that the excited argon atoms play the most important role in the processes of deep decomposition of TMDSN with the formation of silicon atoms and C_2 dimers. The Si–C bonds breaking lead to the formation of the CH_x particles in plasma, in particular, CH_3 , CH , and hydrocarbons. It is assumed in [57] that cyano radical is formed via the reaction of these carbon-containing species with nitrogen under RF discharge. It explains the dependence of the cyano radical band intensity on the nitrogen content in the initial gas mixture (Figure 11f).

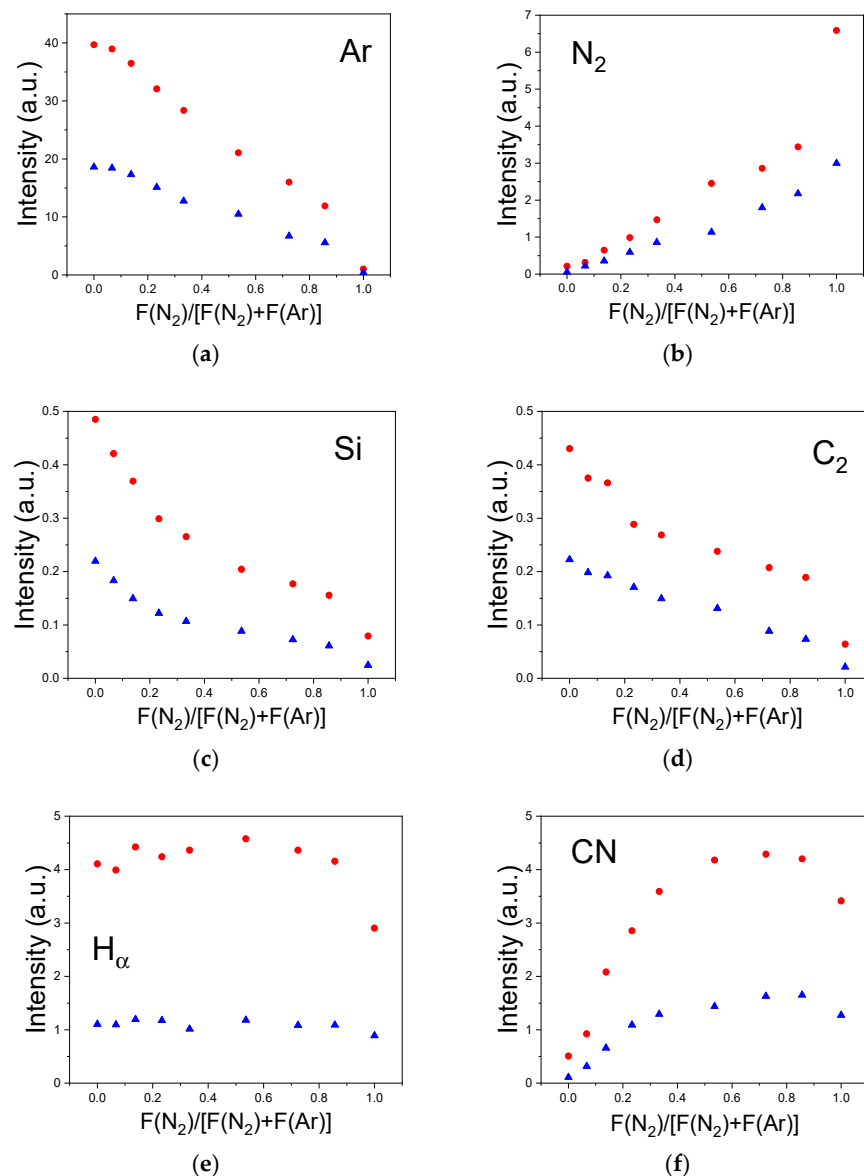


Figure 11. Dependences of the intensities of the argon line at 763.5 nm (a), the nitrogen N_2 band at 357 nm (b), the silicon line at 288.2 nm (c), the C_2 dimer band at 516.5 nm (d), the $H\alpha$ hydrogen line at 656.3 nm (e), the cyano radical CN band at 386.5 nm (f) versus the value of the ratio $R(N_2)$. Triangles—plasma power 200 W, circles—plasma power 400 W.

The mentioned changes in the plasma chemical composition affect the composition of the $SiC_xN_y:H$ films deposited in the ICP CVD processes. The formation of the cyano

radical is correlated with the presence of hydrogen cyanide in the plasma [26,57]. Hydrogen cyanide leaves the reactor and thereby reduces the total amount of carbon in the reactor chamber. The ICP CVD processes for $R(N_2) = 0.4-1$, when a relatively large amount of cyan is formed, give the films with less carbon concentration than in the case of $R(N_2) = 0-0.3$. A slight decrease in the intensity of the cyano radical peak at $R(N_2) = 1$ is likely insufficient for a noticeable change in the elemental composition of the films. However, there is a good agreement between the dependences of Si–C bond content (Figure 8b) and cyano radical intensity (Figure 11f) on $R(N_2)$. An increase in power to 400 W leads to a change in the intensity of all observed lines and bands, but no new lines and bands appear in the spectra (Figure 12).

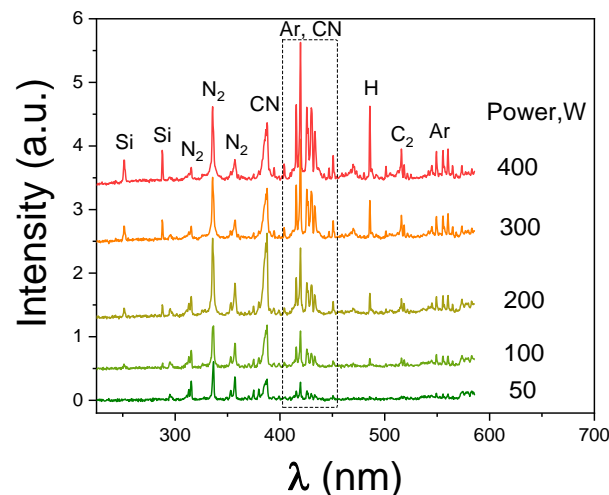


Figure 12. Emission spectra of TMDSN + Ar plasma at different RF discharge powers.

3.5. Functional Characteristics of $a\text{-SiC}_x\text{N}_y\text{:H}$ Films

The above data served as the basis for determining the dependence of the optical (refractive index, transmittance, and bandgap) and mechanical (hardness, Young's modulus, and adhesion to the substrate) characteristics on the conditions of deposition experiments and the chemical composition of the films. The surface properties of $a\text{-SiC}_x\text{N}_y\text{:H}$ films (contact angle, surface free energy) were also studied.

3.5.1. Optical Properties of $a\text{-SiC}_x\text{N}_y\text{:H}$ Films

The optical properties of the films were studied using ellipsometry and spectrophotometry. Figure 13 shows the dependences of the refractive index values on various process parameters such as the pressure of TMDSN, the substrate temperature, the plasma power, and the nitrogen flow rate. The values of n increase with increasing deposition temperatures up to 400 °C reaching $n = 1.98$ in the case of $P(\text{TMDSN}) = 1$ mTorr and $n = 1.82$ at $P(\text{TMDSN}) = 2$ mTorr (Figure 13a). As is known, silicon carbide and silicon nitride have refractive indices equal to 2.6 and 2.0, respectively. With an increase in the deposition temperature of the films, according to the EDX data, the content of silicon and carbon increases and IR spectroscopy confirms an increase in the amount of Si–C bonds, which could lead to an increase in n value. In work [16], a similar dependence was found. The increase in plasma power did not have a significant effect on the refractive index.

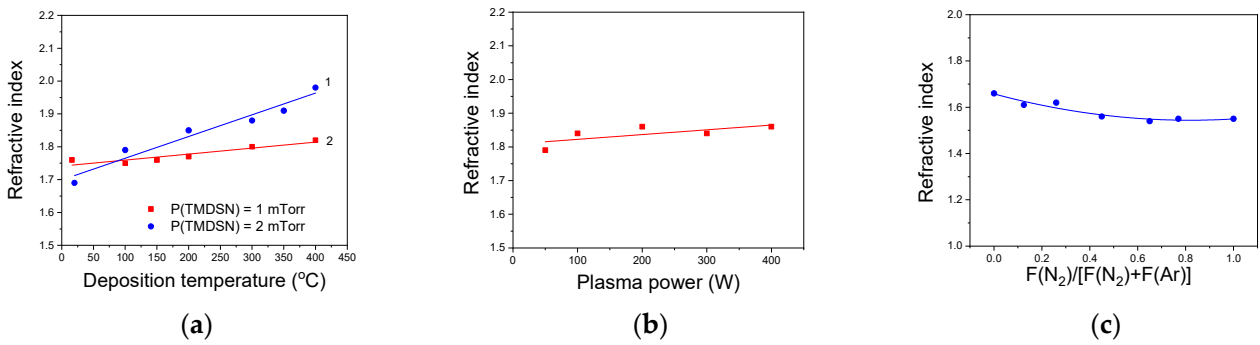


Figure 13. Refractive index of $\text{SiC}_x\text{N}_y\text{:H}$ films as function of (a) the deposition temperature (series B and C); (b) plasma power (series D), and (c) the value of the ratio $R(\text{N}_2)$ (series F).

The optical properties of the a- $\text{SiC}_x\text{N}_y\text{:H}$ films were studied with UV-Vis-NIR spectroscopy using a double beam spectrophotometer in the wavelength range of 190–3200 nm. Figure 14 shows the transmittance spectra of the films of series B, D, and F. It may be observed that the transmittance yield of all the samples reaches 90%–98%.

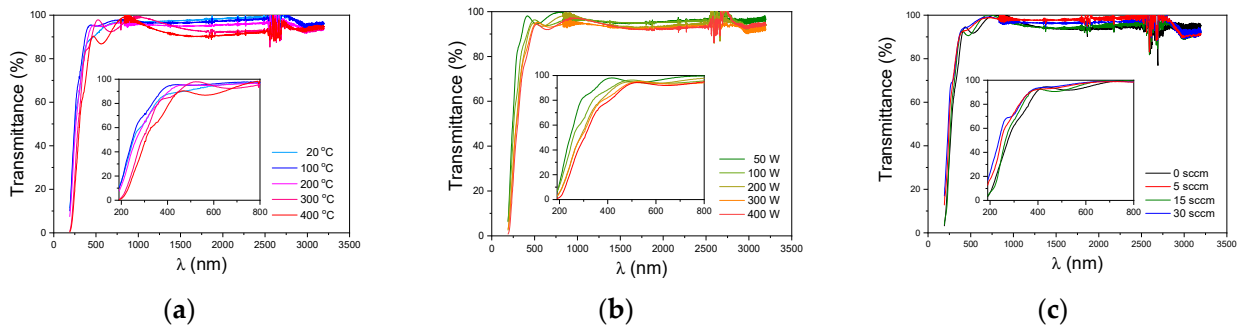


Figure 14. Transmittance spectra of a- $\text{SiC}_x\text{N}_y\text{:H}$ films deposited at different (a) deposition temperature (series B); (b) plasma power (series D), and (c) nitrogen flow rate (series F).

The values of the band gap were determined from Tauc’s plot [58]. The values of the band gap decreased in the range 3.5–2.9 eV and 3.2–2.6 eV with an increase in the film synthesis temperature and in the plasma power, respectively (Figure 15a,b). The values of E_g of samples deposited from TMDAS + Ar + N_2 mixture increased from 3.1 to 3.5 eV with increasing nitrogen flow rate. The values of the band gap obtained for the abovementioned samples are in the range of the values reported in the literature [1,3].

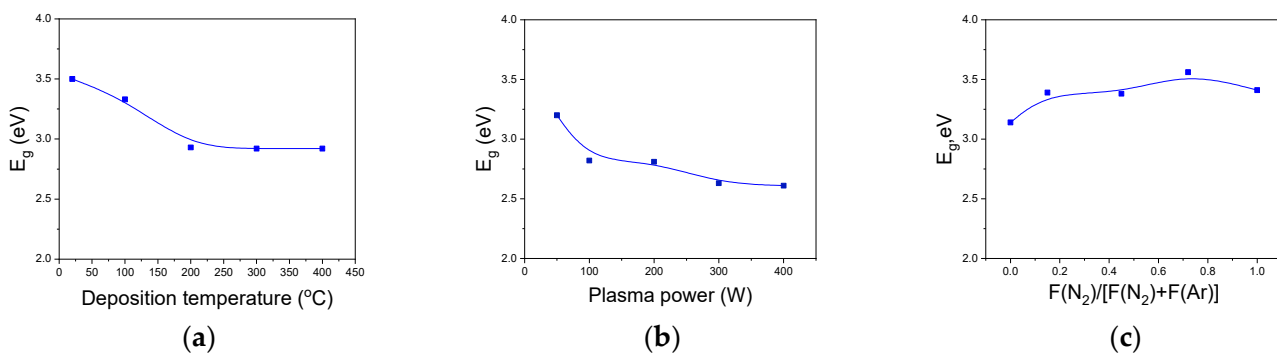


Figure 15. The optical band gap of $\text{SiC}_x\text{N}_y\text{:H}$ films as function of (a) the deposition temperature (series B); (b) plasma power (series D); and (c) the value of the ratio $R(\text{N}_2)$ (series F).

3.5.2. Mechanical Properties of Films

The hardness and elastic modulus of the obtained samples, determined by the nanoindentation method, vary in the range 3.3–13.6 GPa and 57.8–106.4 GPa, and their values increase with an increase in the substrate temperature (Table 6). As noted above, an increase in T_{dep} promoted an increase in the content of Si–C bonds, which led to an increase in the hardness of the films [16]. According to literature data, the maximum hardness value was 36 GPa for films obtained from TMDSN, but these films were deposited at higher temperatures [3,23]. The increase in plasma power also contributed to an increase in the hardness of the films.

Table 6. Mechanical properties of a-SiC_xN_y:H films.

Deposition Conditions							
P(TMDSN), Torr	F(Ar), sccm	F(N ₂), sccm	T _{dep} , °C	P, W	H, GPa	E, GPa	R, %
1 × 10 ⁻³	30	0	20	200	3.33	57.83	41.14
			100		3.46	52.12	41.87
			200		4.65	61.33	47.49
			300		9.20	78.45	62.30
			350		12.09	99.77	70.52
			400		13.57	106.43	66.68
1 × 10 ⁻³	30	0	200	50	5.25	50.36	47.05
				100	3.75	38.54	47.67
				200	4.65	61.33	47.49
				300	5.44	61.37	46.99
				400	10.28	89.88	53.47

3.5.3. Wettability of a-SiC_xN_y:H Films

The wettability of a-SiC_xN_y:H film was evaluated by measuring the contact angle (CA) of two test liquids (water and diethylene glycol), followed by calculating the free energy of the surface. The value of the contact angles of wetting was measured in the sessile drop mode. The water and diethylene glycol wettability of the SiC_xN_y:H films was assessed as film deposition parameters. As shown in Figure 16a,b, an increase in the deposition temperature did not have a significant effect on the value of the contact angle. The water contact angle was approximately 70°. An increase in plasma power from 50 to 400 W led to a decrease in the contact angle from 78° to 62°. All surfaces were found to be hydrophilic because the water contact angle was always less than 90°.

The calculation of the free surface energy (E_s), as well as its polar and dispersion components (E_s^d and E_s^p , respectively), was carried out using three methods. For this, the values of the contact angles of two test liquids (water and diethylene glycol) with different polarities were used. The calculation results are shown in Tables 7 and 8.

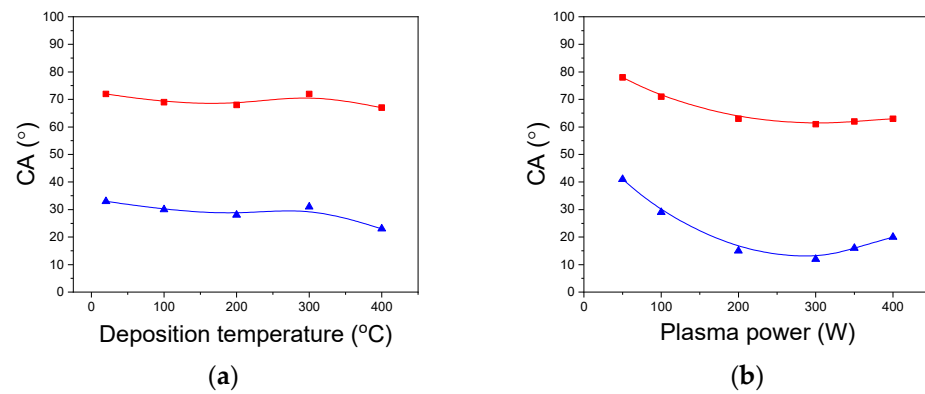


Figure 16. (a) Contact angles as function of deposition temperature (series B). (b) Contact angles as function of plasma power (series D). Test liquids are water (square) and diethylene glycol (triangle).

Table 7. Values of surface free energy as function of film deposition temperature.

T _{dep} , °C	Neumann Method	Owens-Wendt Method			Wu Method		
	E _s , mN/m	E _s ^d , mN/m	E _s ^p , mN/m	E _s , mN/m	E _s ^d , mN/m	E _s ^p , mN/m	E _s , mN/m
20	40 ± 3	27 ± 3	12 ± 2	39 ± 4	25 ± 2	17 ± 2	42 ± 4
100	42 ± 2	27 ± 2	14 ± 1	40 ± 3	25 ± 2	19 ± 2	44 ± 4
200	43 ± 3	27 ± 3	14 ± 2	41 ± 4	26 ± 3	19 ± 3	45 ± 4
300	40 ± 2	28 ± 2	11 ± 1	39 ± 2	26 ± 2	17 ± 2	43 ± 3
400	43 ± 3	29 ± 2	14 ± 1	42 ± 3	27 ± 2	19 ± 2	46 ± 3

Table 8. Values of surface free energy as function of plasma power.

Plasma Power, W	Neumann Method	Owens-Wendt Method			Wu Method		
	E _s , mN/m	E _s ^d , mN/m	E _s ^p , mN/m	E _s , mN/m	E _s ^d , mN/m	E _s ^p , mN/m	E _s , mN/m
50	37 ± 2	26 ± 2	10 ± 1	35 ± 2	23 ± 2	15 ± 2	38 ± 3
100	41 ± 1	28 ± 1	11 ± 1	40 ± 2	26 ± 1	17 ± 2	43 ± 2
200	46 ± 2	29 ± 2	16 ± 1	45 ± 2	28 ± 2	21 ± 2	49 ± 3
300	47 ± 2	28 ± 2	18 ± 2	46 ± 2	28 ± 2	22 ± 2	50 ± 3
350	46 ± 2	28 ± 1	17 ± 1	45 ± 2	28 ± 1	22 ± 1	49 ± 2
400	46 ± 1	27 ± 1	17 ± 1	44 ± 1	27 ± 1	21 ± 1	48 ± 3

3.6. Aging Behavior of a-SiC_xN_y:H Films

A known problem with the use of thin films is that films usually undergo compositional changes upon storage after deposition. A limited number of works dealt with the aging processes of a-SiC_xN_y:H films. In this work, the effect of the film growth conditions on post-deposition stability and oxidation was studied for films obtained using two different initial gas mixtures. The pressure of TMDSN in the reactor chamber was 2 mTorr, the deposition temperature was 200 °C, and plasma power was 200 W. The aging of the films was examined by exposing the samples to air environments. Figure 17 presents the data of element composition and FTIR spectra for SiCN-A and SiCN-N films deposited from TMDSN + Ar (F_{Ar} = 30 sccm) and TMDSN + N₂ (F_{N2} = 30 sccm) mixtures, respectively, during long aging in air. This illustrates that the oxygen uptake is dependent on the conditions of the film formation. The element composition of the SiCN-A film changed insignificantly during the first hours of storage and then remained stable for a long time. The composition of the SiCN-N film changed significantly: the amount of nitrogen decreased and the amount of oxygen increased with an almost constant content of silicon and carbon (Figure 17a,b). Thus, the incorporation of significant amounts of oxygen in SiCN-N film during aging in the air was observed.

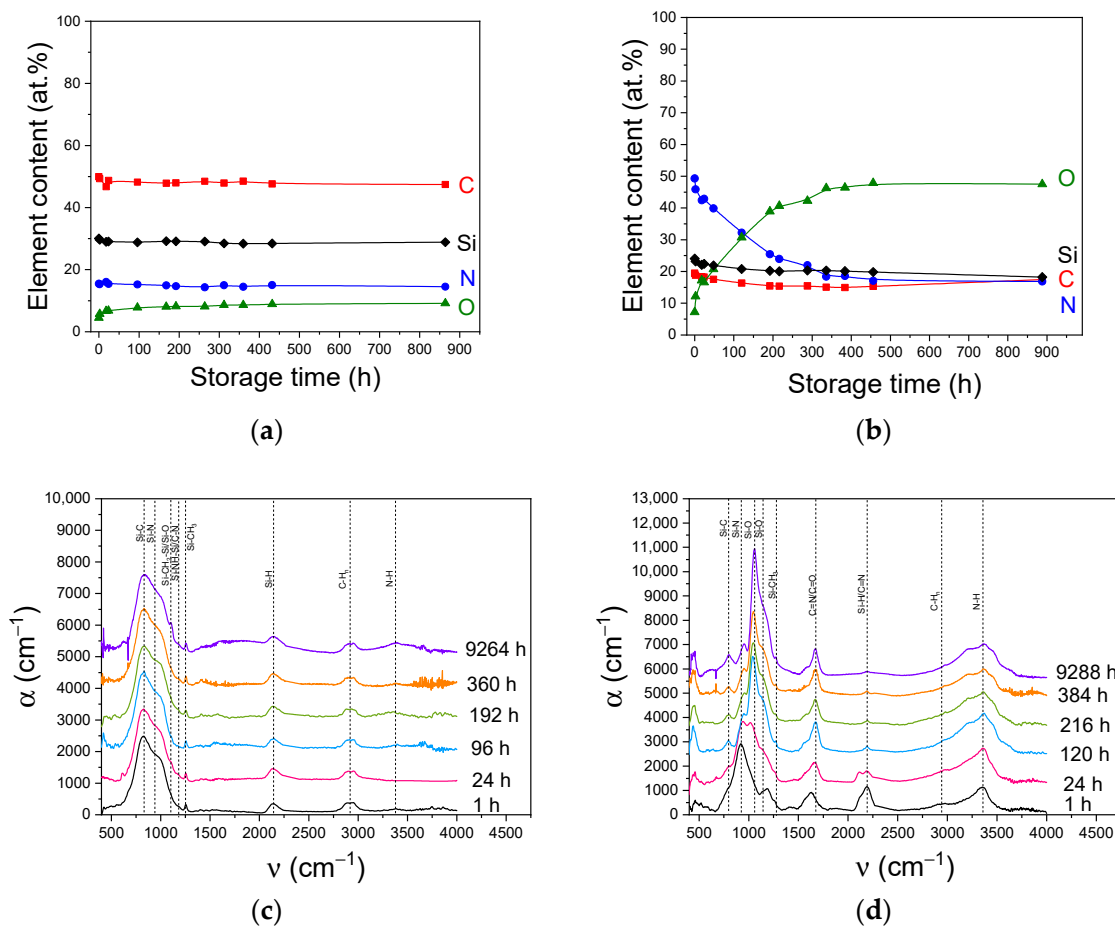


Figure 17. Time dependence of element composition and FTIR spectra of films. Samples SiCN-A (a,c) and SiCN-N (b,d).

The evolution of the FTIR spectra of these samples is shown in Figure 17c,d. The spectrum of SiCN-A film does not change, while the spectrum of SiCN-N film changes significantly. After long-term storage, this spectrum contains three separate bands in the region of 1300–600 cm⁻¹, two of which are weak at 800 cm⁻¹ (Si–C) and 945 cm⁻¹ (Si–N), and one strong at 1040 cm⁻¹ with a shoulder at 1130 cm⁻¹, which correspond to the stretching vibrations of Si–O–Si bonds. The nature of the spectrum change is confirmed by the above data (Figure 17b). The absorption band at 2190 cm⁻¹ disappears, which means the disappearance of Si–H/C≡N groups. There is an increase in the intensity and broadening of the band at 3360 cm⁻¹, possibly due to the appearance of –OH groups. According to [59] the formation of –OH and Si–O–Si groups and the decay of Si–H groups are general trends in the structural changes of the plasma polymers investigated that resulted from aging. In another study, Gengenbach et al. [29] observed the loss of silazane groups and the formation of siloxane cross-links during the oxidative aging of HMDSN polymer.

The influence of the aging process on wettability was also investigated for a-SiC_xN_y:H films (Figure 18 and Table 9). A sharp increase in the water contact angles was observed during the initial stage of aging for both films. However, the film deposited from the nitrogen mixture showed an increase in contact angle by 10°. In this case, the aging process increased the hydrophobicity of the surface, as revealed by an increase in the contact angle of water. The contact angle of a film synthesized from an argon mixture decreased slightly. After several days the water contact angles reach a constant value for both films.

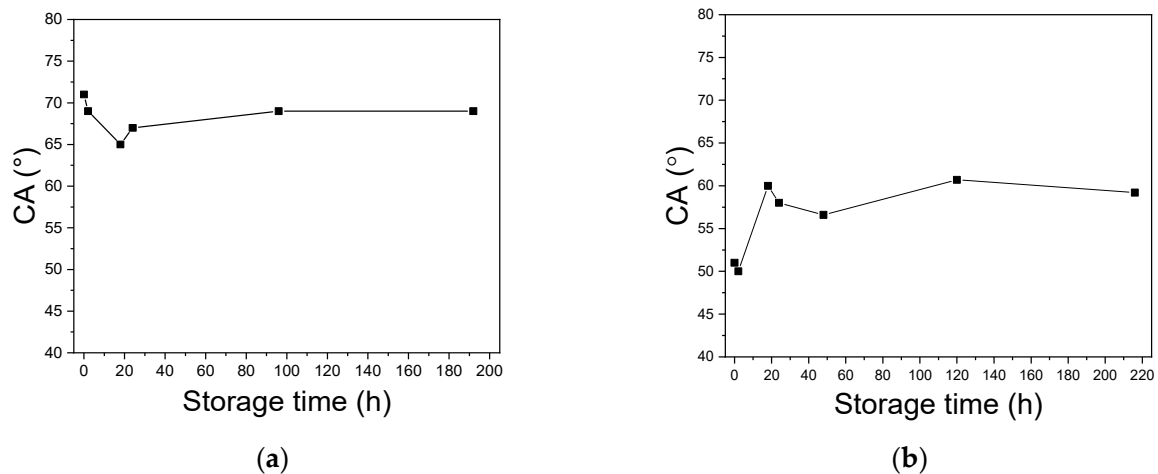


Figure 18. Time dependence of contact angles for films deposited using TMDSN + Ar (a) and TMDSN + N₂ (b) mixture.

Table 9. Values of surface free energy as function of storage time.

Initial Gas Mixture	Aging	Neumann Method	Owens-Wendt Method			Wu Method		
		E_s , mN/m	E_s^d , mN/m	E_s^p , mN/m	E_s , mN/m	E_s^d , mN/m	E_s^p , mN/m	E_s , mN/m
TMDSN + Ar	1 h	41 ± 1	24 ± 1	16 ± 1	40 ± 2	24 ± 1	20 ± 1	44 ± 2
	120 h	41 ± 2	28 ± 1	13 ± 1	41 ± 2	26 ± 1	18 ± 2	46 ± 2
TMDSN + N ₂	1 h	49 ± 2	23 ± 1	28 ± 2	51 ± 2	27 ± 2	29 ± 2	55 ± 3
	120 h	45 ± 2	26 ± 2	19 ± 2	45 ± 3	27 ± 2	23 ± 2	49 ± 3

4. Conclusions

The modern strategies for plasma-enhanced chemical vapor deposition of silicon carbonitride thin films and coatings involve the use of organosilicon volatile compounds as single-source precursors. These compounds already have bonds established between the elements that will comprise the film prior to deposition. Amorphous SiC_xN_y:H films were prepared by using the mixtures of 1,1,3,3-tetramethyldisilazane and Ar or Ar-N₂ via the ICP CVD approach. Through the series of studies, the influence of deposition parameters on the film growth rate, composition, chemical bonding, some functional properties, and film stability was probed. The film properties can be influenced via TMDSN partial pressure, deposition temperature, plasma power, and additional gases. Functional properties, such as refractive index, optical band gap, hardness, and the contact angle, can be tuned by adjusting the parameters of the ICP CVD process. In the entire range of the studied film growth conditions, highly transparent films were obtained.

Special attention was paid to studying the stability of the films. Films were deposited under identical conditions (precursor, deposition temperature, plasma power, and ratio of precursor to additional gas in initial gas mixture). The difference between these two samples was the use of various additional gases. The aging of films was found to be dependent on the type of additional gas. A change in the composition of the samples was observed immediately after they were removed from the reactor chamber. However, for the film obtained from the TMDSN + Ar mixture, it was insignificant, and, in the future, its composition remained constant. In contrast, a film prepared from a mixture with nitrogen underwent significant compositional changes. The nitrogen content dropped sharply, and the oxygen content increased. After about two weeks, the composition of this film stabilized. According to FTIR data, almost all silazane moieties were lost and substantial amounts of oxygen incorporated, mainly in the form of siloxane links.

Supplementary Materials: The following are available online at <https://www.mdpi.com/article/10.3390/coatings12010080/s1>: Figure S1, XRD pattern of SiC_xN_y film. The film deposition conditions: P(TMDSN) = 1 × 10^{−3} Torr, T_{dep} = 200 °C, W = 200 W, F(Ar) = 30 sccm, F(N₂) = 0 sccm.; Table S1, The surface free energy (surface tension) and its components for test liquids of different polarity (T = 25 ± 2 °C, P = 750 Torr).

Author Contributions: M.N.C., film syntheses, investigation, writing—original draft preparation; V.S.S., investigation, writing—original draft preparation; V.R.S., investigation; A.N.K., investigation; M.N.K., investigation; I.V.Y., investigation; M.L.K., methodology, writing—original draft preparation, review and editing, funding acquisition, and project supervisor. All authors contributed to the discussion and interpretation of the results. All authors have read and agreed to the published version of the manuscript.

Funding: This work was supported by the Russian Foundation for Basic Research (RFBR-BRICS Grant No. 18-53-80016). Study of optical properties and film aging process was supported by the Ministry of Science and Higher Education of the Russian Federation in the framework of the Grant No. 121031700314-5.

Institutional Review Board Statement: Not applicable.

Informed Consent Statement: Not applicable.

Data Availability Statement: Not applicable.

Acknowledgments: The authors thank B.A. Kolesov for Raman spectroscopy study, A.A. Shapovalova for FTIR spectroscopy characterization, and E.N. Ermakova for useful discussion.

Conflicts of Interest: The authors declare no conflict of interest.

References

1. Ermakova, E.; Kosinova, M. Organosilicon compounds as single-source precursors for SiCN films production. *J. Organomet. Chem.* **2022**, *958*, 122183. [[CrossRef](#)]
2. Hoffmann, P.; Fainer, N.; Kosinova, M.; Baake, O.; Ensinger, W. Chapter 21. Compilation on Synthesis, Characterization and Properties of Silicon and Boron Carbonitride Films. In *Silicon Carbide—Materials, Processing and Applications in Electronic Devices*; Mukherjee, M., Ed.; InTech: Rijeka, Croatia, 2011; pp. 487–546. ISBN 9789533079684.
3. Fainer, N.I. From Organosilicon Precursors to Multifunctional Silicon Carbonitride. *Russ. J. General Chem.* **2012**, *82*, 43–52. [[CrossRef](#)]
4. Li, Q.; Chen, C.; Xu, M.; Wang, Y.; Wang, X.; Zhang, Z.; Zhao, W.; Stiens, J. Blue-violet emission of silicon carbonitride thin films prepared by sputtering and annealing treatment. *Appl. Surf. Sci.* **2021**, *546*, 149121. [[CrossRef](#)]
5. Zhang, S.; Li, Y.; Yang, H.; Meng, Q.; Wang, W.; Li, H.; Huang, C.; Nishimura, A.; Li, J.; Li, L. Multifunctional Superhydrophobic Composite Coatings with Remarkable Passive Heat Dissipation and Anticorrosion Properties. *Ind. Eng. Chem. Res.* **2021**, *60*, 11019–11029. [[CrossRef](#)]
6. Sundaram, K.; Alizadeh, Z.; Todi, R.; Desai, V. Investigations on hardness of RF sputter deposited SiCN thin films. *Mater. Sci. Eng.* **2004**, *368*, 103–108. [[CrossRef](#)]
7. Wrobel, A.M.; Kryszewski, M.; Gazicki, M. Mechanism of polysilazane thin film formation during glow discharge polymerization of hexamethylcyclotrisilazane. *Polymer* **1976**, *17*, 673–677. [[CrossRef](#)]
8. Gazicki, M.; Wrobel, A.M.; Kruszewski, M. Studies on soluble fraction of glow-discharge polysilazane formed from hexamethylcyclotrisilazane. *J. Appl. Polym. Sci.* **1977**, *21*, 2013–2019. [[CrossRef](#)]
9. Wróbel, A.M.; Kryszewski, M. Effect of glow discharge conditions on structure and thermal properties of polysilazane thin films. *J. Macromol. Sci. Chem. A* **1978**, *12*, 1041–1054. [[CrossRef](#)]
10. Hirotsu, T. Some surface properties of plasma polymers prepared from hexamethyldisilazane and diethylaminotrimethylsilane. *Appl. Polym.* **1979**, *24*, 1957–1964. [[CrossRef](#)]
11. Voronkov, M.G.; Sulimin, A.D.; Yachmenev, V.V.; Mirskov, R.G.; Kokin, V.N.; Chernova, V.G. Production of silicon-nitride films from hexamethylcyclotrisilazane in a high-frequency glow-discharge. *Dokl. Akad. Nauk SSSR* **1981**, *259*, 1130–1132.
12. Bielinski, D.; Wrobel, A.M.; Walkiewicz-Pietrzykowskab, A. Mechanical and tribological properties of thin remote microwave plasma CVD a-Si:N:C films from a single-source precursor. *Tribol. Lett.* **2002**, *13*, 71–76. [[CrossRef](#)]
13. Wróbel, A.M.; Błaszczuk, I.; Walkiewicz-Pietrzykowska, A.; Tracz, A.; Klemberg-Sapieha, J.E.; Aoki, T.; Hatanaka, Y. Remote hydrogen–nitrogen plasma chemical vapor deposition from a tetramethyldisilazane source. Part 1. Mechanism of the process, structure and surface morphology of deposited amorphous hydrogenated silicon carbonitride films. *J. Mater. Sci.* **2003**, *13*, 731–737.

14. Wróbel, A.M.; Błaszczak, I.; Walkiewicz-Pietrzykowska, A.; Bieliński, D.M.; Aoki, T.; Hatanaka, Y. Silicon Carbonitride Films by Remote Hydrogen-Nitrogen Plasma CVD from a Tetramethyldisilazane Source. *J. Electrochem. Soc.* **2004**, *151*, C723–C730. [[CrossRef](#)]
15. Błaszczak-Lezak, I.; Wrobel, A.M.; Aoki, T.; Nakanishi, Y.; Kucinska, I.; Tracz, A. Remote nitrogen microwave plasma chemical vapor deposition from a tetramethyldisilazane precursor. 1. Growth mechanism, structure, and surface morphology of silicon carbonitride films. *Thin Solid Films* **2006**, *497*, 24–34. [[CrossRef](#)]
16. Błaszczak-Lezak, I.; Wrobel, A.; Bieliński, D. Remote nitrogen microwave plasma chemical vapor deposition from a tetramethyldisilazane precursor. 2. Properties of deposited silicon carbonitride films. *Thin Solid Films* **2006**, *497*, 35–41. [[CrossRef](#)]
17. Wrobel, A.M.; Błaszczak-Lezak, I.; Walkiewicz-Pietrzykowska, A. Silicon Carbonitride thin-film coatings fabricated by remote hydrogen–nitrogen microwave plasma chemical vapor deposition from a single-source precursor: Growth process, structure, and properties of the coatings. *J. Appl. Polym. Sci.* **2007**, *105*, 122–129. [[CrossRef](#)]
18. Wrobel, A.M.; Błaszczak-Lezak, I. Remote hydrogen microwave plasma CVD of silicon carbonitride films from a tetramethyldisilazane source. Part 1: Characterization of the process and structure of the films. *Chem. Vap. Depos.* **2007**, *13*, 595–600. [[CrossRef](#)]
19. Wrobel, A.M.; Błaszczak-Lezak, I. Remote Hydrogen Microwave Plasma CVD of Silicon Carbonitride Films From a Tetramethyldisilazane Source. Part 2: Compositional and Structural Dependencies of Film Properties. *Chem. Vap. Depos.* **2007**, *13*, 601–608. [[CrossRef](#)]
20. Wrobel, A.M.; Uznanski, P. Hard silicon carbonitride thin-film coatings produced by remote hydrogen plasma chemical vapor deposition using aminosilane and silazane precursors. 1: Deposition mechanism, chemical structure, and surface morphology. *Plasma Processes Polym.* **2021**, *18*, e2000240. [[CrossRef](#)]
21. Wrobel, A.M.; Uznanski, P. Hard silicon carbonitride thin-film coatings by remote hydrogen plasma chemical vapor deposition using aminosilane and silazane precursors. 2: Physical, optical, and mechanical properties of deposited films. *Plasma Processes Polym.* **2021**, *18*, e2000241. [[CrossRef](#)]
22. Guruvenket, S.; Andrie, S.; Simon, M.; Johnson, K.W.; Sailer, R.A. Atmospheric-Pressure Plasma-Enhanced Chemical Vapor Deposition of a-SiCN:H Films: Role of Precursors on the Film Growth and Properties. *ACS Appl. Mater. Interfaces* **2012**, *4*, 5293–5299. [[CrossRef](#)]
23. Fainer, N.I.; Golubenko, A.N.; Rumyantsev, Y.u.M.; Kesler, V.G.; Maximovskii, E.A.; Ayupov, B.M.; Kuznetsov, F.A. Synthesis of Silicon Carbonitride Dielectric Films with Improved Optical and Mechanical Properties from Tetramethyldisilazane. *Glass Phys. Chem.* **2013**, *39*, 77–88. [[CrossRef](#)]
24. Sobczyk-Guzenda, A.; Oleśko, K.; Gazicki-Lipman, M.; Szymański, W.; Balcerzak, J.; Wendler, B.; Szymanowski, H. Chemical structure and optical properties of a-SiNC coatings synthesized from different disilazane precursors with the RF plasma enhanced CVD technique—A comparative study. *Mater. Res. Express* **2019**, *6*, 016410. [[CrossRef](#)]
25. Szymanowski, H.; Oleśko, K.; Kowalski, J.; Fijałkowski, M.; Gazicki-Lipman, M.; Sobczyk-Guzenda, A. Thin SiNC/SiOC coatings with a gradient of refractive index deposited from organosilicon precursor. *Coatings* **2020**, *10*, 794. [[CrossRef](#)]
26. Belmahi, M.; Bulou, S.; Thouvenin, A.; de Pouques, L.; Hugon, R.; Le Brizoual, L.; Miska, P.; Geneve, D.; Vasseur, J.-L.; Bougdira, J. Microwave Plasma Process for SiCN:H Thin Films Synthesis with Composition Varying from SiC:H to SiN:H in H₂/N₂/Ar/Hexamethyldisilazane Gas Mixture. *Plasma Processes Polym.* **2014**, *11*, 551–558. [[CrossRef](#)]
27. Jiang, L.; Tian, H.; Li, J.; Xiang, P.; Peng, Y.; Wang, T.; Hou, P.; Xiao, T.; Tan, X. The influence of NH₃ flow rate on the microstructure and oxidation properties of a-Si-C-N:H films prepared by PECVD technology. *Appl. Surf. Sci.* **2020**, *513*, 145861. [[CrossRef](#)]
28. Huber, C.; Stein, B.; Kalt, H. Plasma-enhanced chemical vapor deposition of amorphous silicon carbonitride: Deposition temperature dependence of bonding structure, refractive index, mechanical stress and their aging under ambient air. *Thin Solid Films* **2017**, *634*, 66–72. [[CrossRef](#)]
29. Gengenbach, T.R.; Griesser, H. Post-deposition ageing reactions differ markedly between plasma polymers deposited from siloxane and silazane monomers. *Polymer* **1999**, *40*, 5079–5094. [[CrossRef](#)]
30. Sukhanov, Y.N.; Ershov, A.P.; Rudenko, K.V.; Orlikovsky, A.A. Comparative study of inductively coupled and microwave BF₃ plasmas for microelectronic technology applications. In Proceedings of the Micro- and Nanoelectronics 2003, Zvenigo-rod, Russia, 28 May 2004; pp. 55–64.
31. Zhang, Y.; Tang, J.; Hu, Y.; Yuan, J.; Guan, L.; Li, X.; Cui, X.; Ding, G.; Shi, X.; Xu, K.; et al. Effect of hydrogen content on dielectric strength of the silicon nitride film deposited by ICP-CVD. *Chin. Phys. B* **2021**, *30*, 048103. [[CrossRef](#)]
32. Wu, H.-Y.; Hsu, C.-H.; Liu, T.-X.; Ou, Y.-C.; Hsu, Y.-H.; Wu, W.-Y.; Lien, S.-Y.; Jiang, Y.-L. Silicon nitride cover layer prepared by silane-free plasma chemical vapor deposition for high quality surface passivation of silicon solar cells. *Surf. Coat. Technol.* **2019**, *376*, 68–73. [[CrossRef](#)]
33. Bang, S.-H.; Suk, J.-H.; Kim, K.-S.; Park, J.-H.; Hwang, N.-M. Effects of radio frequency power and gas ratio on barrier properties of SiO_xN_y films deposited by inductively coupled plasma chemical vapor deposition. *Thin Solid Films* **2019**, *669*, 108–113. [[CrossRef](#)]
34. Qiu, P.; Wu, B.; Fu, P.; Li, M.; Xie, Y.; Kan, Q. Fabrication and Characterization of Low-Threshold Single Fundamental Mode VCSELs With Dielectric DBR Mirror. *IEEE Photonics J.* **2021**, *13*, 1500106. [[CrossRef](#)]
35. Mundo, R.D.; d’Agostino, R.; Fracassi, F.; Palumbo, F. A Novel organosilicon source for low temperature plasma deposition of silicon nitride-like thin films. *Plasma Processes Polym.* **2005**, *2*, 612–617. [[CrossRef](#)]

36. Fainer, N.I.; Kosinova, M.L.; Maximovsky, E.A.; Rumyantsev, Y.M.; Kuznetsov, F.A.; Kesler, V.G.; Kirienko, V.V. Study of the structure and phase composition of nanocrystalline silicon oxynitride films synthesized by ICP-CVD. *Nucl. Instr. Meth. Phys. Res.* **2005**, *543*, 134–138. [[CrossRef](#)]
37. Rumyantsev, Y.M.; Chagin, M.N.; Kosinova, M.L.; Kuznetsov, F.A. Synthesis of thin silicon carbonitride films from hexamethyldisilazane in an inductively coupled plasma reactor. *Inorg. Mater.* **2015**, *51*, 897–902. [[CrossRef](#)]
38. Shayapov, V.R.; Chagin, M.N.; Kolodin, A.N.; Kosinova, M.L. Deposition of Films from a Mixture of Hexamethylcyclotrisilazane Vapor and Argon in Inductively Coupled Plasma. *Glass Phys. Chem.* **2019**, *45*, 525–531. [[CrossRef](#)]
39. Rumyantsev, Y.M.; Chagin, M.N.; Shayapov, V.R.; Yushina, I.V.; Kichai, V.N.; Kosinova, M.L. Synthesis and Properties of Thin Films Formed by Vapor Deposition from Tetramethylsilane in a Radio-Frequency Inductively Coupled Plasma Discharge. *Glass Phys. Chem.* **2018**, *44*, 174–182. [[CrossRef](#)]
40. Orlikovsky, A.A.; Rudenko, K.V.; Averkin, S.N. Fine-Line Plasma-Enhanced Processes on the Basis of a Set of Pilot Units with a Scalable Inductively Coupled Plasma Source for Use in Microelectronics. *High Energy Chem.* **2006**, *40*, 182–193. [[CrossRef](#)]
41. Scofield, J.H. Hartree-Slater subshell photoionization cross-sections at 1254 and 1487 eV. *J. Electron Spectrosc. Relat. Phenom.* **1976**, *8*, 129–137. [[CrossRef](#)]
42. Shirley, D.A. High-Resolution X-Ray Photoemission Spectrum of the Valence Bands of Gold. *Phys. Rev. B* **1972**, *5*, 4709–4714. [[CrossRef](#)]
43. CasaXPS: Processing Software for XPS, AES, SIMS and More. Available online: www.casaxps.com (accessed on 30 December 2021).
44. Pearse, R.W.B.; Gaydon, A.G. *The Identification of Molecular Spectra*; John Wiley and Sons: Hoboken, NY, USA, 1963.
45. Dieke, G.H. *The Hydrogen Molecule Wavelength Tables of Gerhard Heinrich Dieke*; Crosswhite, H.M., Ed.; Wiley-InterScience: New York, NY, USA, 1972; ISBN 0471188905.
46. NIST Atomic Spectra Database; NIST Standard Reference Database 78 Version 5.9. Available online: <https://physics.nist.gov/asd> (accessed on 10 December 2021).
47. Kwok, D.Y.; Neumann, A.W. Contact angle measurements and contact angle interpretation. *Adv. Colloid Interface Sci.* **1999**, *81*, 167–249. [[CrossRef](#)]
48. Owens, D.K.; Wendt, R.C. Estimation of the surface free energy of polymers. *J. Appl. Polym. Sci.* **1969**, *13*, 1741–1747. [[CrossRef](#)]
49. Wu, S. *Polymer Interface and Adhesion*; Marcel Dekker: New York, NY, USA, 1982; ISBN 9780824715335.
50. Vassallo, E.; Cremona, A.; Ghezzi, F.; Dellera, F.; Laguardia, L.; Ambrosone, G.; Coscia, U. Structural and optical properties of amorphous hydrogenated silicon carbonitride films produced by PECVD. *Appl. Surf. Sci.* **2006**, *252*, 7993–8000. [[CrossRef](#)]
51. Bellamy, L.J. *The Infrared Spectra of Complex Molecules*; Springer: London, UK, 1980; ISBN 9780412223501.
52. Anderson, D.R. Chap. 10. Infrared, Raman, and Ultraviolet Spectroscopy. In *Analysis of Silicones*; Smith, A.L., Ed.; Wiley-Interscience: New York, NY, USA, 1974.
53. Rao, C.N.R. *Chemical Applications of Infrared Spectroscopy*; Academic Press: New York, NY, USA, 1963.
54. Launer, P.J.; Arkles, B. Infrared analysis of organosilicon compounds: Spectra-structure correlations. In *Silicon Compounds: Silanes & Silicones*; Gelest, Inc.: Morrisville, PA, USA, 2013; pp. 175–178.
55. Tolstoy, V.P.; Chernyshova, I.V.; Skryshevsky, V.A. *Handbook of Infrared Spectroscopy of Ultrathin Films*; Wiley-Interscience: Hoboken, NY, USA, 2003; ISBN 047135404X.
56. Ferrari, A.C.; Robertson, J. Interpretation of Raman spectra of disordered and amorphous carbon. *Phys. Rev. B* **2000**, *61*, 14095–14107. [[CrossRef](#)]
57. Jamroz, P.; Zyrnicki, W. Spectroscopic study of the decomposition process of tetramethylsilane in the N₂-H₂ and N₂-Ar low pressure plasma. *Diam. Relat. Mater.* **2005**, *14*, 1498–1507. [[CrossRef](#)]
58. Tauc, J.; Menth, A. States in the gap. *J. Non-Cryst. Solids* **1972**, *8*, 569–585. [[CrossRef](#)]
59. Wrobel, A.M. Aging process in plasma-polymerized organosilicon thin films. *J. Macromol. Sci.-Chem.* **1985**, *22*, 1089–1100. [[CrossRef](#)]